IEEE Access
Multidisciplinary | Rapid Review | Open Access Journal

Date of publication xxxx 00, 0000, date of current version xxxx 00, 0000.

Digital Object Identifier 10.1109/ACCESS.2017.Doi Number

Evaluation of the ICP algorithm in 3D point cloud registration

Peng Li[1, 3], Ruisheng Wang[2, 3], Yanxia Wang[1], and Wuyong Tao[4]

[1]School of Geographic Information and Tourism, Chuzhou University, Chuzhou 239000 China
[2]School of Geographical Sciences, Guangzhou University, Guangzhou 510006 China
[3]Department of Geomatics Engineering, University of Calgary, Calgary T2N 1N4 Canada
[4]School of Geodesy and Geomatics, Wuhan University, Wuhan 430079, China

Corresponding author: Ruisheng Wang (e-mail: ruiswang@ucalgary.ca) and Peng Li (Peng.Li2@ucalgary.ca).

This work was supported by the Key Research Project of Anhui Provincial Department of Education (Grants KJ2018A0425 and KJ2019A0633). This work is also supported by the Foreign Visiting and Training Program for Young Talents in Colleges and Universities of Anhui Province (Grant gxgwfx2019057) and the Research Project of Chuzhou University (Grant 2019qd04).

ABSTRACT The iterative closest point (ICP) algorithm is widely used in three-dimensional (3D) point cloud registration, and it is very stable and robust. However, its biggest drawback is being easily trapped in a local optimal solution, which results in the incorrect registration result. Currently, there is neither a clear effective range to define whether the ICP algorithm will fall into a local optimum nor a study providing a comprehensive evaluation of the ICP algorithm. In this paper, we take the overlap ratio, angle, distance, and noise as the influencing factors of ICP and evaluate the validity, robustness, accuracy, and efficiency of point-to-point and point-to-plane ICP by using four datasets. We first analyze the effective ranges of the two ICP algorithms with respect to overlap ratio, angle, and distance and then propose a universal effective range for the three factors. Next, the effect of Gaussian noise on the validity and accuracy of two ICPs is evaluated. We also analyze the factors influencing ICP accuracy and explain their changing rules. We finally study the effect of different parameters on the efficiency. All results are compared by using point-to-point and point-to-plane ICP algorithms. The results show that the overlap ratio has no effect on validity, but it has a significant influence on accuracy. The angle has a great impact on the validity and efficiency of ICP but has no effect on accuracy. The distance only affects validity, has a limited effect on efficiency and no effect on accuracy. Meanwhile, Gaussian noise has a little effect on the validity. In addition, the general effective range of point-to-point ICP is larger than that of point-to-plane ICP, but the point-to-plane ICP algorithm presents a better efficiency. The point-to-point ICP is more robust to Gaussian noise with respect to validity, while the point-to-plane is more resistant in terms of accuracy.

INDEX TERMS ICP, Point Cloud, Registration, Validity, Accuracy, Efficiency

I. INTRODUCTION

The ICP algorithm [1] has long been regarded as the most classic algorithm in point cloud data registration, and it has been widely used for many years. The biggest advantage of ICP is that the results are very stable and robust. However, the shortcomings are also obvious, for example, the computational efficiency is too low, the overlap ratio of the two datasets is high, the convergence domain is narrow, and it is easy to fall into a local optimal solution [2]. Over the years, many researchers have been working on perfecting ICP, including improving the efficiency of the ICP algorithm, increasing the accuracy of the algorithm and solving the problem of local optimal solutions.

Improving the efficiency of the ICP algorithm is mainly achieved by reducing the number of points participating in the operation [3], increasing the search speed of the nearest neighbor [4], improving the reliability of the established point correspondence [5], registering multiview point sets [6], and reducing the number of iterations [7], which has achieved relatively obvious results. After each iteration of ICP, the distance between the nearest neighbor in the two datasets is calculated so that the point-to-point correspondence can be judged. Therefore, the fewer the points participating in the search, the less the calculation time will be. Most of this linking is done by point cloud simplification or down sampling. The main methods of

This article has been accepted for publication in a future issue of this journal, but has not been fully edited. Content may change prior to final publication. Citation information: DOI 10.1109/ACCESS.2020.2986470, IEEE Access

down sampling are uniform sampling [8], random sampling [9], and feature-based sampling [10]. Since the ICP algorithm considers the nearest neighbor of the target dataset to be the corresponding point of the source dataset, the search method of the nearest neighbor affects the efficiency of the algorithm. In the early days, the approach was mainly based on the global search method, but this method is extremely inefficient. With the generation of data structures such as KD tree and octree, the nearest neighbor problem is introduced in point cloud data processing [11, 12], which greatly accelerates the search and improves the efficiency of ICP. Another efficiency improvement is to speed up the convergence and reduce the number of iterations, which requires an increase in the accuracy of the search for the point-to-point correspondence. The current methods mainly include judgment criteria based on point-to-line [13] and point-to-plane [14] and adding feature information of the points to the criteria [15]. These methods can improve the convergence speed of ICP to a certain extent.

From the aspect of algorithm precision optimization, the main focus is on the solution method of the rigid body transformation matrix. The traditional method of 3D coordinate transformation is least squares (LS) [16]. Moreover, the methods of total least squares (TLS) [17, 18], weighted total least squares (WTLS) [19-21], and robust weight total least squares (RWTLS) [22, 23] have been proposed to solve problems such as the coefficient matrix, gross error, and more.

In solving the issue of ICP falling into a local optimal solution, the process is different from the improvements in efficiency and precision. The research on improving the efficiency and accuracy belongs to the optimization of the algorithm, and the problem of solving a local optimal solution is to avoid the wrong result. Once the registered point cloud falls into a local optimal solution, the registration result is wrong.

To solve this problem, the most common solution at present is to divide the registration process of the point cloud into two phases. First, the two datasets are roughly aligned by global registration (or coarse registration), and then local registration (or fine registration) is done by using ICP. This method solves the initial position problem of ICP by global registration and can effectively avoid the problem of local optimal solution. The study of global registration mainly focuses on two aspects: point feature descriptors and search strategies for correspondences.

The point feature descriptor uses a series of values to describe the local shape around a point, which can be used to distinguish the differences between each point. By setting a criterion, a small number of points with significant features can be selected. This makes it easier to search for point-to-point correspondence in two datasets, improving the search efficiency. The existing descriptors are Spin Image (SI) [24], 3D Shape Context (3DSC) [25], Signature of Histogram of OrienTations (SHOT) [26,27], Unique Shape Context (USC) [28], Point Feature Histogram (PFH) [29], Fast Point Feature Histogram (FPFH) [30], Rotation Projection Statistics (RoPS) [31], Local Surface Patch (LSP) [32], Tri-Spin-Image (TriSI) [33] and so on. On the other hand, a search strategy is used to find the point-to-point correspondence between the two datasets. The existing methods are RANdom SAmpling Consistency (RANSAC) [34], robust global registration [35], Greedy Initial Alignment (GIA) [30], 4-Point Coplanar (4PCS) [36], Four Initial Point Pairs (FIPP) [37], Evolutionary Calculation [38], etc. Global registration is currently the best way to solve the problem of ICP falling into a local optimum.

However, two questions have been ignored over the years in the study of global registration and local registration, which is when must global registration be performed first and under what circumstances ICP can obtain the correct registration result without global registration? In general, there are three main factors that affect ICP as to whether there is a local optimal solution, which is the overlap ratio, the angle and the distance between the two datasets. Many studies have mentioned that the higher the overlap ratio of the two datasets is, the more accurate the result is. However, at present, it has not been verified that the ICP algorithm is effective or reliable within a specific range of overlap ratios. Similarly, when the angle between the two datasets is greater than a specific number and the separation distance is large, ICP will fall into a local optimum, and these problems also have no clear answer.

To solve this problem, in this paper, the three factors of the overlap ratio, angle and distance between the two point cloud datasets are taken as the main research objects, and the correctness of the ICP results is used as the judgment principle. By looking for the law of the results of ICP in different parameters, the parameter range of the validity of the ICP algorithm is obtained, which provides a reference for whether or not to add global registration before performing ICP. In addition, the accuracy and efficiency of different factors are analyzed within the effective range of ICP.

II. ICP ALGORITHM

A. PRINCIPLE OF ICP

The ICP algorithm constructs a rigid transformation matrix by searching the point-to-point correspondence between two datasets and aligns two datasets accurately through iteration. The steps are as follows [39]:

1) Take the point set $p_i \in P$ in the target point cloud P.
2) Search for the corresponding point of p_i in source dataset Q and constitute point-to-point correspondence.
3) Generate a rigid transformation matrix by using point-to-point correspondence and transform the source dataset into a new dataset with the matrix.

This article has been accepted for publication in a future issue of this journal, but has not been fully edited. Content may change prior to final publication. Citation information: DOI 10.1109/ACCESS.2020.2986470, IEEE Access

4) Determine whether the value of $dRMS(P^*, Q^*)$ is less than a threshold (see Equation 1); if greater, go back to step 2 and continue until the convergence conditions are met.

$$dRMS(P^*,Q^*)=\sqrt{\frac{1}{n}\sum_{i=1}^{n}\left(\left\|p_i-q_j\right\|\right)^2}<\sigma,(1\le j\le m) \qquad (1)$$

where q_j is the point in the source dataset corresponding to p_i in the target dataset; n and m are the numbers of P and Q, respectively; and σ is the threshold for the minimum distance between the two datasets. $dRMS(P^*, Q^*)$ is the error equation of the ICP algorithm, which determines whether the iteration of the ICP algorithm continues or stops.

In the above steps, how to determine the point-to-point correspondence affects the iteration process. The current common methods are point-to-point [1] [3-12], point-to-line [13] [40-41], point-to-plane [14] [42-45] and so on. Point-to-point ICP uses the minimum distance of p_i and q_j in the two datasets as the point-to-point correspondence. Because it only depends on the spatial relationship between the points, this method converges slowly during the iteration. Unlike point-to-point ICP, point-to-line ICP uses a linear segmentation method to approximate the actual surface. The distance from the point p_i to the line between its nearest points q_j and q_{j+1}, which is used to simulate the distance from the actual laser point to the surface, is considered the correspondence. The correspondence of point-to-line ICP is more in line with the actual situation, so its convergence speed is faster than that of point-to-point ICP. However, the method is more sensitive to the initial values, which facilitates the fall into a local optimum. The point-to-plane ICP makes full use of the characteristics of the actual surface to filter out the wrong points. It considers the distance from the point p_i to the tangent plane of point q_j as the correspondence. In addition, the normal angle difference of the corresponding point is also used for judgment. This method takes into account both the Euclidean distance and the angle between the normal vectors, so it can exclude some obviously wrong matches in advance, and it has a more accurate solution angle and faster convergence speed.

B. INFLUENCE FACTORS OF ICP

The point cloud registration result based on the ICP algorithm may produce one of two completely different situations: one is to obtain the correct registration result, and the other is to fall into a local optimal solution. In addition, even if the correct registration results are obtained, the accuracy of the results and the time efficiency of the registration process will vary from one factor to another. The factors affecting the results mainly include the overlap ratio, angle, distance, shape of the object, noise and so on. Wherein the overlap ratio indicates the same area ratio between the two point cloud datasets, the angle refers to the angle between the approximate planes formed by two datasets (see Figure 1), the distance is the straight-line distance between the center points of two datasets, and the object shape is the difference in the distribution of points in space.

1) OVERLAP RATIO

Since the ICP algorithm uses the nearest neighbor as the point-to-point correspondence, if the overlap ratio of the two datasets is too low, the accuracy of the registration result is low because the rigid body transformation matrix is solved based on the least squares idea. At the same time, it is also possible that the algorithm may fall into a local optimum because the coincident region is far from the center of gravity of the point cloud. In the collection process of the point cloud dataset, the original point set of the independent object is mostly obtained by rotating one circle around the object, as shown in Figure 1.

The same area of the red and blue arcs in FIG. 1 is the theoretical overlap area of the two datasets, and the sampling angles are different by 20 degrees. If the shape of the horizontal profile of the object is approximately a circle, the overlap ratio can be approximately equal to 88.9%. In reality, the horizontal profiles of most objects are different from a circle, such as: humans, animals, kettles, buildings, etc. Therefore, a certain error is introduced when estimating the overlap ratio.

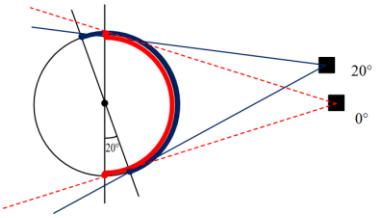

FIGURE 1. Angle-based overlapping area.

$$O=(1-\frac{\theta}{180})\times 100\% \qquad (2)$$

Equation 2 shows the conversion between the overlap ratio and sampling angle, where O is the overlap ratio and θ is the sampling angle. However, the sampling angle can approximate the overlap ratio. On the one hand, the larger the angle, the lower the overlap ratio, and vice versa; on the other hand, the sampling angle index is easier to obtain. In this paper, the overlap ratio of the data is replaced by the sampling angle.

2) ANGLE

The angle is also an important factor affecting the results of ICP registration. Since ICP is an iterative process, on the one hand, the larger the angle of the two datasets is, the more steps are iterated. On the other hand, when the angle increases to a certain threshold, the registration result of the flip may occur, that is, falling into a local optimal solution.

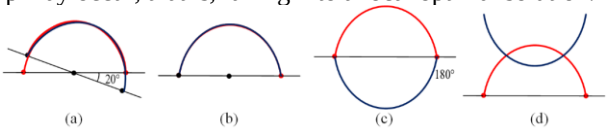

This article has been accepted for publication in a future issue of this journal, but has not been fully edited. Content may change prior to final publication. Citation information: DOI 10.1109/ACCESS.2020.2986470, IEEE Access

FIGURE 2. Schematic results of the registration with different angles: (a) before with 20 degrees, (b) after with 20 degrees, (c) before with 180 degrees, and (d) after with 180 degrees.

Figure 2 shows the initial positions and Schematic results of the registrations with 20 degrees and 180 degrees. When the initial angle is small, ICP gradually moves to the correct position in the correct direction during the iteration, but if the initial angle is too large, the result may be completely flipped. Here, in order to distinguish from the previous sampling angle, the angle is referred to as a rotation angle in the following content.

3) DISTANCE

The distance refers to the linear distance between the center points of two datasets. Since the ICP algorithm constructs the same point pair by searching the nearest neighbor of the target dataset in each iteration, if the distance between two datasets is different in space, the search results may be varied, and in extreme case, it will fall into a local optimal solution. In addition, the direction of the distance between the two points is also likely to have a certain influence on the registration result.

Figure 3 shows the different original locations of two datasets with point-to-point ICP. The results of searching for the nearest neighbor in different positions may have differences, and the process of iteration will also be different, which may result in an erroneous iterative process and a local optimal solution. In this paper, only the laws of parallel and vertical changes are analyzed.

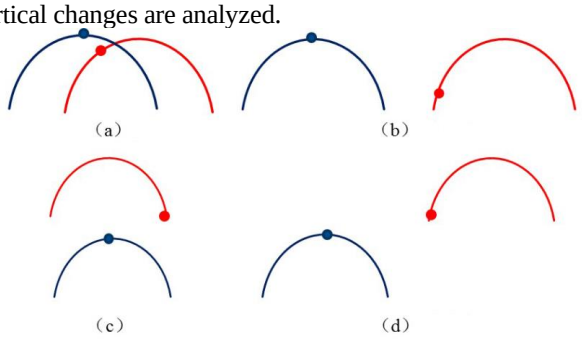

FIGURE 3. Different positions of two datasets with point-to-point ICP: (a) crossing, (b) parallel interval, (c) vertical interval, and (d) diagonal interval.

4) OTHER FACTORS

Other factors may also have an impact on the ICP registration results, such as noise, the shape of the object and so on. Different shapes result in different search locations for the nearest neighbors and have an impact on the ICP iterative process.

In this paper, the influences of the sampling angle, rotation angle and distance parameter on the ICP registration result are emphasized by means of uniform variations of parameter thresholds. The shape of the object is only briefly analyzed.

III. EXPERIMENTAL SETUP

A. DATASETS

To evaluate ICP, four types of datasets were selected for the experiments, which were the Synthetic, Kinect, Stereo, and Laser datasets. Among them, the Synthetic dataset was obtained from the Stanford University Computer Graphics Laboratory (http://graphics.stanford.edu), and the other three datasets were from the Computer Vision Laboratory of the University of Bologna (http://vision.deis.unibo.it/).

1) SYNTHETIC DATASETS

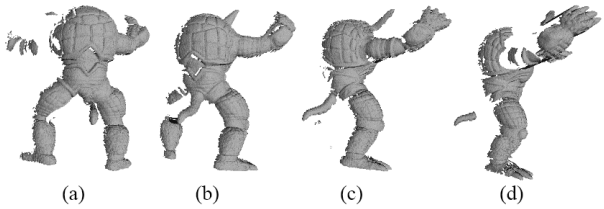

FIGURE 4. Partial original data from Armadillo datasets: (a) 0 degrees, (b) 30 degrees, (c) 60 degrees, and (d) 90 degrees.

Synthetic datasets were obtained by scanning from a graphics scanner, and their name is Armadillo. Seven original datasets were selected for the experiment. Each dataset was acquired from 0 to 180 degrees at intervals of 30 degrees along the outer circumference of the object. Figure 4 shows each Armadillo dataset at 0, 30, 60, and 90 degrees.

2) KINECT DATASETS

The name of the Kinect datasets is Duck, and they were derived from the Kinect camera. Ten original datasets were chosen, which were acquired from 0 to 180 degrees at intervals of 20 degrees. Figure 5 shows the Kinect datasets of 0, 20, 40 and 80 degrees.

FIGURE 5. Partial original data with Duck datasets: (a) 0 degrees, (b) 20 degrees, (c) 40 degrees, and (d) 80 degrees.

3) STEREO DATASETS

The Stereo datasets, whose name is Mario, were collected by space time stereo. There are also 10 original datasets, and the acquisition principle is the same as that of the Kinect datasets. Figure 6 shows the Stereo datasets of 0, 20, 40 and 80 degrees.

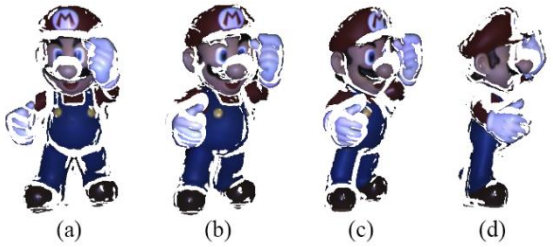

FIGURE 6. Partial original data with Mario datasets: (a) 0 degrees, (b) 20 degrees, (c) 40 degrees, and (d) 80 degrees.

4) LASER DATASETS

The laser point cloud datasets, with the name of Chef, were collected by a laser scanner, and the number of datasets used for the experiments and the selection principle are the same

This article has been accepted for publication in a future issue of this journal, but has not been fully edited. Content may change prior to final publication. Citation information: DOI 10.1109/ACCESS.2020.2986470, IEEE Access

as those for the stereo datasets. Figure 7 shows the laser datasets of 0, 20, 40 and 80 degrees.

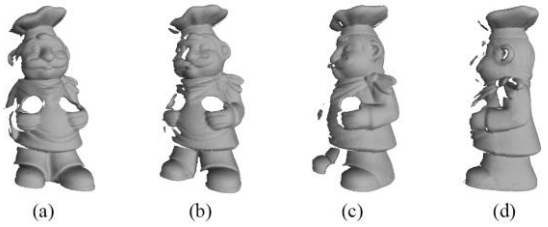

FIGURE 7. Partial original data with Chef datasets: (a) 0 degrees, (b) 20 degrees, (c) 40 degrees, and (d) 80 degrees.

Table 1 shows the comparison of the above four datasets, which were obtained from Synthetic, Microsoft Kinect, SpaceTime stereo and Laser scanner. The nearest neighbor of Chef is the largest among all datasets, the number of which is also the largest. On the premise that the objects are all single objects, the more points available, the better the details can be described. In terms of quality, Chef is the highest, Armadillo is second, Duck is lower, and Mario has the worst quality of the point clouds. The quality of the dataset depends on two aspects, one is the data integrity, and the other is the number of points. In the four types of datasets, Chef is optimal regardless of integrity or number. Mario not only is the worst in continuity but also presents numerous scattered points. The quality of the other two types of datasets is at an intermediate level.

TABLE I
COMPARISON OF FOUR TYPES OF POINT CLOUD DATASETS

Dataset Name	Acquisition	Quality	Occlusion	Clutter	Number of points	Nearest neighbor (m)	Horizontal profile
Armadillo	Synthetic	Medium	N	N	28000	0.0005	Horseshoe
Duck	Microsoft Kinect	Low	N	Y	15000	0.002	Ellipse
Mario	SpaceTime stereo	Very Low	Y	Y	41000	0.1	Ellipse
Chef	Laser scanner	High	Y	N	69000	0.5	Circle

The choice of point cloud datasets is based on three considerations: one is the variety of data acquisition techniques, another is the different data accuracies, and the third is the difference in quality. The above four types of datasets basically represent the current mainstream point cloud data acquisition methods, and the accuracy and quality generally cover the three levels of high, medium and low. The nearest neighbor ranges from 1 mm to 0.5 m, which provides a large span. Therefore, the selection of experimental data has good coverage, and the experimental results also have a certain versatility.

B. DATA PREPROCESSING

1) SAMPLING ANGLE

The above four types of datasets were directly acquired at different sampling angles, so these data are relatively complete. The first dataset in the continuously collected datasets is agreed to be a 0-degree sampling angle, and the remaining datasets are calculated from the angle of 0 degrees. Although the sampling angle cannot be equal to the overlap ratio, there is a certain relationship between them. Table 2 shows the approximate relationship between the overlap ratio and the sampling angle when the horizontal section of the object is approximately circular.

TABLE II
COMPARISON OF POINT CLOUD SAMPLING ANGLE AND OVERLAP RATIO

Armadillo datasets			Duck, Mario, and Chef datasets		
SN	Sampling angle	Overlap ratio (%)	SN	Sampling angle	Overlap ratio (%)
1	0	100	1	0	100
2	30	83.3	2	20	88.9
3	60	66.7	3	40	77.8
4	90	50.0	4	60	66.7
5	120	33.3	5	80	55.6

In the experiment, the 0-degree angle of a dataset is taken as the target dataset, and the others are the source datasets. Under the premise that the rotation angle and distance of all source datasets are identical, the source datasets with different sampling angles in the four types of datasets and the target datasets are executed by the ICP algorithm to find the critical value of ICP.

2) ROTATION ANGLE

There is only one dataset with different sampling angles in the source datasets, so the rotation angles of the source datasets need to be preprocessed. The process is as follows: First, all the datasets with different sampling angles are rotated into a position parallel to the target datasets, which are used as the 0-degree angle; then, they are rotated around the center of the object to 180 degrees at 10-degree intervals.

In the 4 types of datasets, each type is selected for 6 different datasets with different overlap rates (including 0 degrees), and each dataset generates 19 datasets of different rotation angles, for a total of 380 datasets. Figure 8 shows the results of the Duck datasets for 20 sampling degrees from 0 to 180 rotation angles.

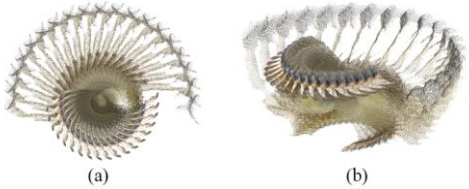

FIGURE 8. Results of Duck datasets at 0 degrees after rotation: (a) Top view and (b) oblique view.

In the experiment, the dataset with a 0-degree sampling angle and 0-degree rotation angle is the target dataset, and the others are the source datasets.

This article has been accepted for publication in a future issue of this journal, but has not been fully edited. Content may change prior to final publication. Citation information: DOI 10.1109/ACCESS.2020.2986470, IEEE Access

3) TRANSLATION

Datasets with a 0-degree sampling angle from the 4 types of data are used for translation processing. There are two translation directions: one is to translate in a direction parallel to the approximate surface of the object, and the other is in a perpendicular direction. The translation interval in both directions is equivalent to the length of the object in that direction. Figure 9 shows the separation distance of the translation, where ΔS_1 and ΔS_2 represent the translation interval for each of the two directions.

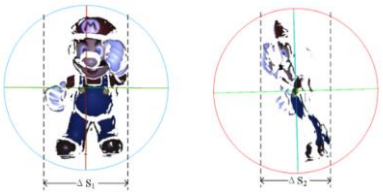

FIGURE 9. Translation intervals of the point cloud dataset in both directions.

To find the effective threshold of the distance, each dataset performs 20 equal-distance translations in two directions, and a total of 160 datasets are generated. The translated 160 datasets are the target datasets, and the rest are the source datasets. Next, the source datasets and the target datasets are verified by the ICP algorithm. Figure 10 shows the translation results of Mario datasets in both directions.

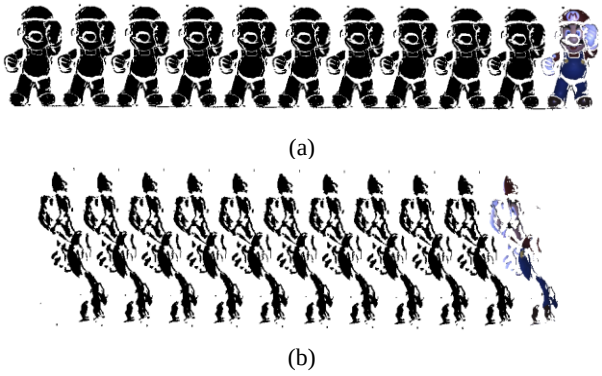

(a)

(b)

FIGURE 10. Partial translation results for 0-degree datasets in Mario datasets: (a) Parallel direction and (b) vertical direction.

4) GAUSSIAN NOISE

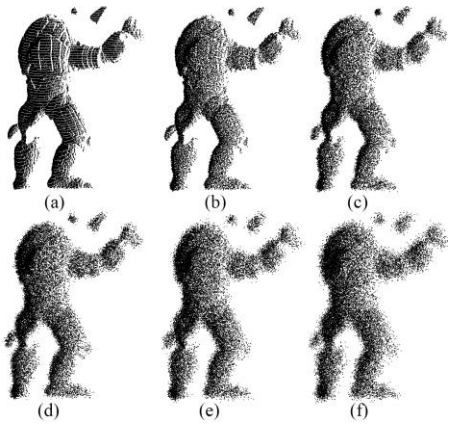

FIGURE 11. Armadillo datasets with different levels of Gaussian noise: (a) No Gaussian noise, (b) Gaussian noise—Level 1, (c) Gaussian noise—Level 2, (d) Gaussian noise—Level 3, (e) Gaussian noise—Level 4, and (f) Gaussian noise—Level 5.

Five levels of Gaussian noise are added to the original datasets with standard deviations of σ, 2σ, 3σ, 4σ and 5σ to each pair of datasets, where σ denotes the sampling distance of points. For a given standard deviation, Gaussian noise is independently added to the x-, y-, and z-axes of each dataset point. Figure 11 illustrates the results of the Armadillo datasets after applying the different levels of Gaussian noise.

The purpose of Gaussian noise is to verify the influence of noise data on the ICP algorithm. The results of ICP with respect to different levels of Gaussian noise are presented in Sect. 4.3.

C. ICP ALGORITHM EXECUTION

In terms of convergence speed, point-to-plane ICP is theoretically the fastest, point-to-line ICP is next, and point-to-point ICP is the slowest. In this paper, point-to-point and point-to-plane ICP algorithms are used for evaluation. The results of point-to-line ICP should be somewhere in between. Both ICP algorithms are evaluated for their effectiveness and efficiency, while the accuracy of registration only considers point-to-point ICP (see Section 3.4.2 for details). Different ICP algorithms can end the iteration by setting the same error threshold, so the same registration datasets can obtain the same or similar registration accuracy.

During the execution of each ICP, the evaluation of the results is performed under the condition that one influencing factor changes uniformly while the other parameters remain unchanged. Among the datasets, the sampling angle is uniformly changed according to 0, 30, 60, 90, 120 degrees (Armadillo) or 0, 20, 40, 60, 80, 100 degrees (Duck, Mario and Chef), while maintaining the same rotation angle and distance. The rotation angle increases uniformly from 0 to 180 degrees at 10-degree intervals, and the distance increases from 0 to 20 in multiples of the coordinate range of the object. In addition, different levels of Gaussian noise datasets are also used in the experiments while keeping the three parameters constant.

D. EVALUATION CRITERIA

We test four datasets in terms of validity, robustness, accuracy and efficiency. Each evaluation criterion is tested separately by using two ICP algorithms except for accuracy. Their definitions are given in the following.

1) VALIDITY

In this study, the validity of ICP is based on three factors: the overlap ratio, angle and distance, expressed in terms of sampling angle, rotation angle and distance, respectively. The basis for determining the validity includes two aspects, one is to compare the value of $dRMS(P^*, Q^*)$ after the iteration is terminated, and the second is to make a manual judgment by superimposing two datasets after registration. There are only two cases of registration based on ICP: correct and wrong. Under the premise of the source dataset, even if the values of the sampling angle, rotation and distance are different, the

This article has been accepted for publication in a future issue of this journal, but has not been fully edited. Content may change prior to final publication. Citation information: DOI 10.1109/ACCESS.2020.2986470, IEEE Access

values of *dRMS*(*P**, *Q**) must be the same or similar once the registration result is correct. In contrast, if the result is wrong, ICP mostly falls into a local optimal solution. In this case, the position of the source dataset after registration is very different from the correct result, and the value of *dRMS*(*P**, *Q**) between the two is also quite different. In the process of continuous change of the parameter threshold, when the value is abrupt, the registration result with the mutation is highly likely to fall into a local optimal solution. Then, manual judgment is performed for verification by visually displaying the two datasets after registration. The purpose of the validity evaluation is to find the threshold ranges of three parameters in which the ICP algorithm can obtain the correct registration. When the parameter value is increased to a specific value resulting in an incorrect registration, the parameter threshold is considered to be ineffective. Even if the registration is correct as the parameter threshold increases again, it is considered that the ICP algorithm is unstable in this range and is not included in the validity range of the parameter.

2) ROBUSTNESS

There may be noise, occlusion, outliers in the dataset used for registration, whose effects on the results indicate the robustness of ICP. In fact, when the ICP algorithm searches the point-to-point correspondences, the farthest point pairs can be filtered out by setting the distance threshold. Therefore, outliers have no effect on the ICP algorithm. The effect of occlusion on ICP is also limited. Because ICP uses the least squares method to solve the rigid transformation matrix. If the occluded points occupy a small proportion in the entire dataset, the result has little effect. If the ratio is too large, it is more appropriate to attribute the problem to the overlap ratio.

In this paper, Gaussian noise is used to evaluate the robustness of the ICP algorithm. The five levels of Gaussian noise datasets are executed by using two ICP algorithms in order to evaluate their validity on three parameters. Then, by comparing the validity difference between the Gaussian noise and non-Gaussian noise datasets, the robustness of the two ICP algorithms is evaluated.

3) ACCURACY

The value of *dRMS*(*P**, *Q**) is usually used to evaluate the registration accuracy, however, there is a problem. Different datasets have different sampling intervals (the nearest neighbor), which makes them incomparable. To solve the comparability of error between different sampling intervals, the relative *dRMS*(*P**, *Q**) is introduced (see Equation 1). The relative *dRMS*(*P**, *Q**) (Expressed by $dRMS^2_R(P^*, Q^*)$) eliminates the difference between different sampling intervals on the basis of the objective function, and its value represents a multiple of the nearest neighbor. The formula is as follows:

$$dRMS^2_R(P^*,Q^*)=\frac{dRMS^2(P^*,Q^*)}{S^2} \tag{3}$$

where *P** and *Q** represent the nearest neighbor pairs in the two datasets and S is the length of the nearest neighbors.

Another problem is that if two datasets with a low overlap ratio are correctly registered together, the value of $dRMS^2_R(P^*, Q^*)$ is not necessarily the smallest (see the left of Figure 12). Conversely, although the value $dRMS^2_R(P^*, Q^*)$ is small and the position is very close, the error may be greater if the overlap ratio is low (see the right of Figure 12).

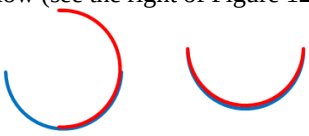

FIGURE 12. Registration results of two datasets with 50% overlap, left: Correct position; right: Wrong position.

In figure 12, the left is the correct position after registration, but the result of ICP is most likely as shown in the right. The reason for this is that the $dRMS^2_R(P^*, Q^*)$ value of the right is less than that of the left. In addition to $dRMS^2_R(P^*, Q^*)$, in this section, the accuracy evaluation adds another expression, the true error. The true error, which is manually measured, is the selection of several point-to-point correspondences after registration and the calculation of the error value. The formula of the true error is as follows:

$$E_R(P^*,Q^*)=\frac{\sum_{k=1}^{m}\left(\left\|q_k-p_k\right\|\right)}{m\cdot s} \tag{4}$$

In the above formula, q_k and p_k are the *k*-th same point pair in two datasets, *m* is the number of selected points, and *s* is the sampling interval distance of the points.

It should be noted that the accuracy evaluation is only performed within the effective range of ICP, and the case of a local optimal solution is considered to be incorrectly registered and is not considered. Meanwhile, the accuracy evaluation is only for the correct registration result. The rotation angle and distance have no effect on the accuracy of the correct result. Therefore, the accuracy evaluation is mainly used for the registration error of datasets with different sampling angles.

4) EFFICIENCY

The efficiency evaluation can be based on the run time or the iterations of ICP. Iteration indicates how many times the ICP algorithm has been run, and the run time counts the execution time of the ICP algorithm, including reading point cloud dataset, finding point-to-point correspondences, calculating rigid transformation matrices, etc. In this paper, the run time is used to evaluate the efficiency of the ICP algorithm with different parameters. Furthermore, to eliminate the impact of different points on the run time, the relative run time is used instead of the run time. The relative run time is the ratio of the run time to the number of points. When comparing the efficiency of point-to-point and point-to-plane ICP, the number of iterations is selected instead of the relative run time. This is because the number of iterations can more accurately describe the difference between the two ICP algorithms.

This article has been accepted for publication in a future issue of this journal, but has not been fully edited. Content may change prior to final publication. Citation information: DOI 10.1109/ACCESS.2020.2986470, IEEE Access

IV. RESULTS ANALYSIS

A. VALIDITY OF POINT-TO-POINT ICP

1) VALIDITY BASED ON SAMPLING ANGLE - ROTATION ANGLE

To verify the registration results of two datasets with different sampling angles and rotation angles, we uniformly use the dataset with 0-degree sampling angle and 0-degree rotation angle as the target dataset. The other datasets are used as the source datasets, including sampling angles of 0 degrees, and the datasets are uniformly rotated by 10 degrees. The ICP algorithms are executed between the target and the source datasets. Figure 13 shows the values of $dRMS^2_R(P^*, Q^*)$ after each registration.

In the figure, the abscissa indicates different rotation angles, and the ordinate is the value of $dRMS^2_R(P^*, Q^*)$. The curves of different colors indicate the sampling angles. It can be seen from the figure that the registration results of the four datasets with the sampling angle-rotation angle parameters have certain similarities.

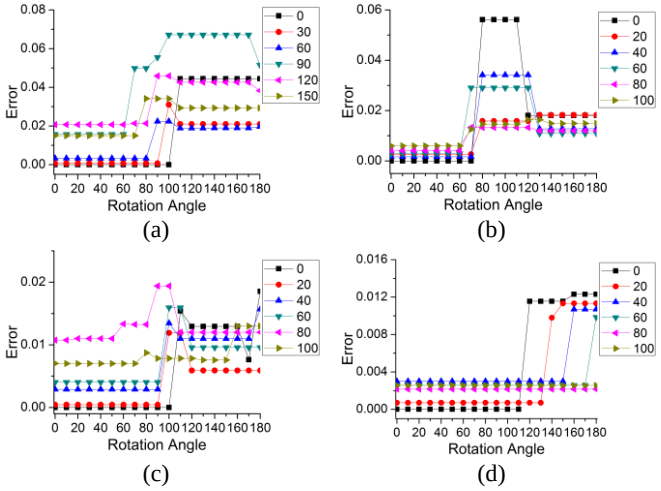

FIGURE 13. Registration errors with the sampling angle-rotation angle: (a) Armadillo, (b) Duck, (c) Mario, and (d) Chef.

First, the values of $dRMS^2_R(P^*, Q^*)$ are initially stabilized at a lower value. When the rotation angles are increased to a specific value, the $dRMS^2_R(P^*, Q^*)$ values exhibit a mutation, and the two values before and after the mutation have a large difference. This law is the same for the four datasets. According to the evaluation criteria in Section 3.4, it can be preliminarily believed that the registration results before the mutation are correct, and results of the mutation are trapped in a local optimal solution. For the occurrence of an abrupt change, the manual interpretation is used for verification. Figure 14 shows the registration results of datasets with a sampling angle of 30 in the Armadillo datasets at several rotation angles, where a has a rotation angle of 90, b is 100 degrees, and c is 110 degrees, corresponding to the three points of discontinuity on the orange line in Figure 14a.

It can be seen from figures 13 and 14 that the datasets with a sampling angle of 30 degrees have consistent values of $dRMS^2_R(P^*, Q^*)$ when the rotation angle is less than 90 degrees. It is reasonable to believe that in the above case, the ICP algorithm can achieve the correct registration result in the range of 90 degrees or less by comparing with Figure 13a. When the rotation angle is more than 90 degrees, the value is abrupt and larger than the correct registration result. Referring to Figure 14, these registration results are wrong. When the rotation angle is more than 90 degrees, ICP will fall into a local optimal solution. Therefore, the rotation angle has a valid range beyond which the registration result is wrong. In addition, the values of 100 and 110 degrees are different. From figure 14 b and c, both fall into a local optimal solution. This suggests that the results of a local optimum based on ICP may not be unique. In practice, the types of local optima are mostly between 1 and 4, and the value depends on the shape of the object and the sample angle.

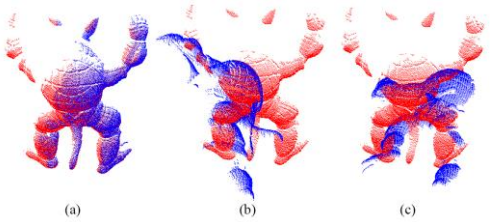

FIGURE 14. Results of correct registration and local minima: (a) Correct registration, (b) local minima one, and (c) local minima two.

For the sampling angle, as it increases, the values of the results in the four types of datasets are generally increased at first and then decreased. This shows that when the sampling angle is too large, the registration result shown in Figure 12 is very likely to occur. That is, on the surface it appears that the values decrease, but the errors increase instead. Concurrently, the differences between the correct and wrong values tend to decrease. This is because the larger the sampling angle, the smaller the overlap ratio of the registration point set and the target point set, and therefore, the registration error is greater.

On the other hand, there are some differences in the results of the four datasets. First, the critical values of the rotation angle in each dataset are varied. Figure 15a shows the critical values based on the sampling angle – rotation angle. The critical values of the rotation angles in the Armadillo point cloud vary from 60 to 100 degrees with the sampling angle, between 60 and 70 in Duck, between 70 and 100 in the Mario, and between 110 and 180 in the Chef datasets. Except for the Chef datasets, the critical values in the other three types of datasets are relatively close, and they decrease slowly as the sampling angles increase. For the Chef datasets, the critical values of the rotation angle tend to increase with the sampling angle. This is because the shape of the object of the Chef dataset is similar to that of a cylinder, whose horizontal profile approximates a circle. In the same way, the horizontal profiles of datasets acquired at each sampling angle are similar to an arc. Thus, the situation in figure 12 appears. That is, the closer the horizontal profile is to an arc, the higher the critical value of the rotation angle, but the

This article has been accepted for publication in a future issue of this journal, but has not been fully edited. Content may change prior to final publication. Citation information: DOI 10.1109/ACCESS.2020.2986470, IEEE Access

greater the error. The other three types of datasets do not have this phenomenon because their horizontal profiles are irregular.

Furthermore, the critical sampling angle, at which the value curves start to fall as a whole, is different in the four datasets. The Armadillo is 120 degrees, while Duck, the Mario and Chef are 100, 80, 40 degrees, respectively. Since the registration error increases with the sampling angle, this relationship indicates that the registration result error growth rate at the sampling angle becomes larger when the value curves start to fall. The critical value of the sampling angle indicates the ability of different data to resist error, which is affected by the object's shape and the data integrity. Among the four types of data, the Armadillo datasets have the highest sampling angle threshold, while the shape is the least close to a cylinder, and the data continuity is the worst.

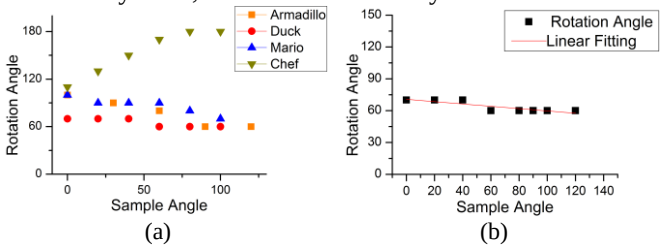

FIGURE 15. Effective range fitting based on sample angle-rotation angle: (a) Effective critical point of each dataset and (b) universal effective range fitting.

To find the universal effective range of ICP based on the sampling angle-rotation angle in different types of point cloud datasets, the minimum values of the critical points in the four datasets are extracted and linearly fitted to obtain the red line shown in Figure 15b. When located below the red line, the ICP has a higher probability of not falling into a local optimal solution, and vice versa. It can be seen from the figure that the sampling angle has little effect on whether the ICP falls into a local optimum. Even when the overlap ratio of the two datasets is less than 50%, they can still be aligned together, but the accuracy changes greatly. The rotation angle has a significant influence on ICP. There is a critical value for the angle of rotation, and the algorithm must fall into a local optimum when it exceeds this threshold. It should be noted that the line in figure 15 is the result obtained under the premise that the initial positions of the two datasets substantially overlap, that is, the range of the fit is the best result under the premise that the distance parameters do not affect ICP. The effects of the distance parameters on the registration results are shown in the following two sections.

2) VALIDITY BASED ON SAMPLING ANGLE - DISTANCE

This section mainly evaluates the effect of the sampling angle and distance on ICP registration results. The target datasets are uniformly translated 20 times at regular intervals along the approximate planes parallel and perpendicular to the datasets. The rotation angles of the source datasets are adjusted to be 0 degrees to the target datasets, and the registration results in the two directions are as shown in Figures. 16 and 19.

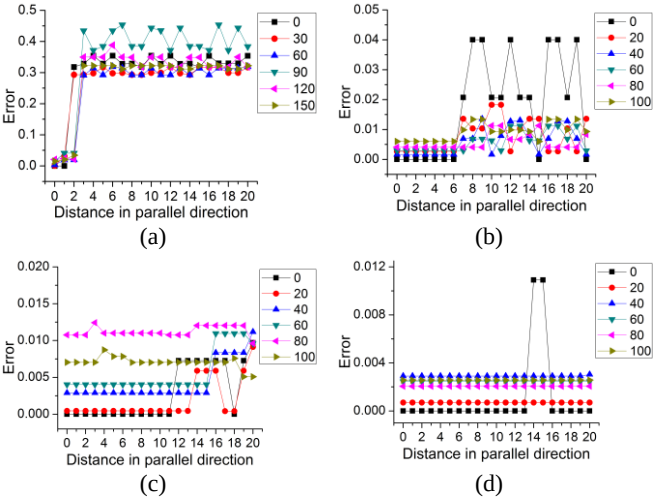

FIGURE 16. Registration errors with sampling angle-distance along the parallel direction: (a) Armadillo, (b) Duck, (c) Mario, and (d) Chef.

Figure 16 presents the registration results when the target datasets are translated in the parallel direction, where the abscissa is a multiple of the translation, the ordinate is the $dRMS^2_R(P^*, Q^*)$ value, and the legend is a different sampling angle. In the figure, the effective distances of different datasets in the parallel direction are very different. The Armadillo datasets are the smallest, which are all less than twice the translation separation distance. The Duck datasets are second and between 6-10 times. The Mario datasets are large and 11-15 times within 60 degrees of the sampling angle. The Chef datasets have the largest effective distance, which is more than 20 times except for the cases of 14- and 15-times distances when the sampling angle is 0 degrees.

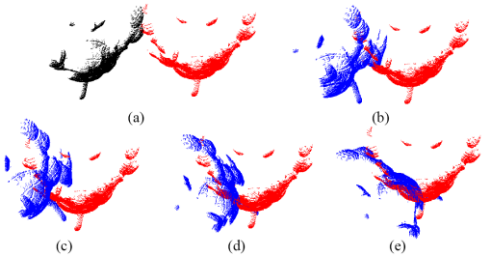

FIGURE 17. ICP iterative process of Armadillo datasets: (a) Original position, (b) 1 iteration, (c) 3 iterations, (d) 10 iterations, and (e) 20 iterations.

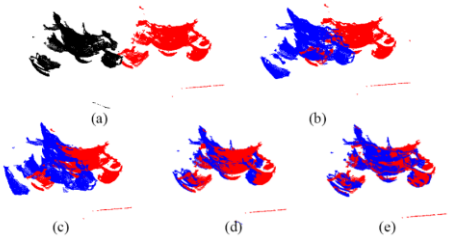

FIGURE 18. ICP iterative process of Mario datasets: (a) Original position, (b) 1 iteration, (c) 3 iterations, (d) 10 iterations, and (e) 20 iterations.

The most common cause of the above differences is the difference in the shape of the dataset object. ICP is iteratively transformed by finding the nearest neighbor, so the difference in object shape will result in different search

This article has been accepted for publication in a future issue of this journal, but has not been fully edited. Content may change prior to final publication. Citation information: DOI 10.1109/ACCESS.2020.2986470, IEEE Access

results for the nearest neighbor (Refer to Figure 3). Taking the two types of datasets of the Armadillo and Mario as an example, the object of the Armadillo dataset is Armadillo, whose horizontal section is shaped such as a horseshoe, while the Mario is approximately trapezoidal and is named SuperMarin. Figures 17 and 18 are the ICP iterative processes for the two datasets, where the sampling angles are 30 degrees for the Armadillo and 20 degrees for the Mario, the horizontal offsets are both 1 time, and the rotation angles are both 0 degrees. In the figure, the red datasets are the target datasets, black are the source datasets, and blue are the results of the source after each iteration.

As seen from the above two figures, the source dataset of the Mario gradually becomes parallel to the target dataset during the iterative process, while the Armadillo shows some rotation after the first iteration. The cause of these phenomena is that the difference in the shape of the objects causes the search results of the nearest neighbors to be different, and thus, the rigid transform matrix generated after each iteration is greatly deviated.

Additionally, beyond the effective range, the $dRMS^2_R(P^*, Q^*)$ values of most datasets swing up and down considerably, as seen from figure 16. Even the result of the previous unit distance falls into a local optimum, and the latter unit is correct. This indicates that the distance has a large effect on the results of ICP. Moreover, in addition to the correct results within the valid range, the results outside the effective range are highly biased.

Figure 19 shows the registration results when the target datasets are translated in the direction perpendicular to the plane of the object, where the horizontal and vertical coordinates and the meaning of the legend are consistent with those in figure 16.

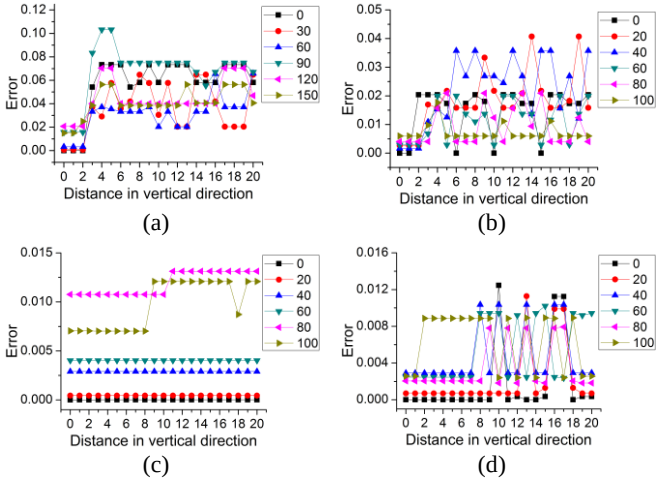

FIGURE 19. Registration errors with sampling angle-distance along the vertical direction: (a) Armadillo, (b) Duck, (c) Mario, and (d) Chef.

The results in the vertical direction are different from those in the parallel. Relative to the parallel direction, the effective ranges of the Armadillo and the Mario are increased in the vertical direction, while being reduced in the datasets of the Duck and the Chef. The target dataset of the Armadillo is symmetrical in the vertical direction, which makes the search of the nearest neighbor more accurate with respect to the parallel direction. The Mario datasets have many outliers and occlusions, and there are certain point-to-point correspondences in the outliers between different point sets, which makes the search efficiency for the nearest neighbors increase. The Duck and Chef datasets are continuous and asymmetrical. As the vertical distance increases, the probability of the wrong nearest neighbor is also greatly increased. Outside the effective range, the amplitude and frequency of the up and down swings in the results of the vertical translation are significantly higher than those in the horizontal direction, which indicates that the stability in the vertical direction is worse than that in the horizontal direction.

Figure 20 shows the effective ranges of the four datasets based on the sampling angle-translation multiple in both directions.

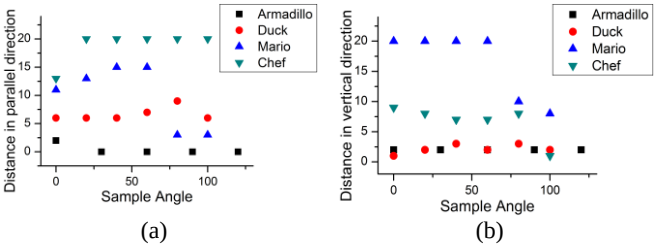

FIGURE 20. Effective critical point of each dataset based on the sampling angle-distance: (a) Parallel direction and (b) vertical direction.

In general, the curves of the effective ranges are relatively flat in the four datasets. This result indicates that the effect of the sampling angle on ICP effectiveness is limited, while the translation distance has a greater impact. In the four datasets, the effective range of the Armadillo is the smallest, and the Duck is second. The Chef and the Mario have the largest effective distance in the horizontal and vertical directions, respectively. According to the principle of universality, the minimum ranges of all datasets in two directions are selected to construct the universal effective range of sampling angle-distance, as shown in Figure 21.

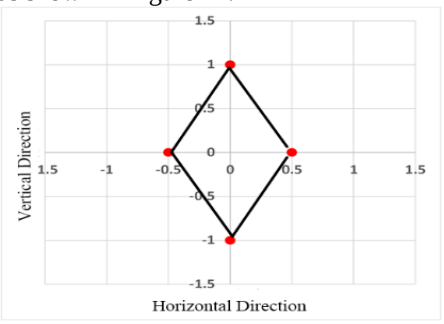

FIGURE 21. Universal effective range fitting based on the sample angle-distance.

Since most of the Armadillo datasets fall into a local optimum after a 1-time distance, a set of experiments is performed with a horizontal distance of 0.5 times. These experiments all achieved correct results, so the 0.5-fold unit distance is considered to be the effective range in the horizontal direction.

This article has been accepted for publication in a future issue of this journal, but has not been fully edited. Content may change prior to final publication. Citation information: DOI 10.1109/ACCESS.2020.2986470, IEEE Access

3) VALIDITY BASED ON ROTATION ANGLE-DISTANCE

In the four-point cloud datasets, a Armadillo dataset with a sampling angle of 30 degrees and the other datasets with an angle of 20 degrees are uniformly rotated from 0 degrees at an interval of 10 degrees, which are used as the source datasets. It can be seen from Section 4.1.1 that the effective range of ICP based on the sampling angle-rotation angle is less than 60 degrees, so the maximum rotation angle of the source datasets above is 60 degrees. Meanwhile, the selection principle of the target datasets is the same as that of the experiment based on the sampling angle-distance (Section 4.1.2). Figures 22 and 23 are the registration results when the target datasets are translated in the parallel and vertical directions, wherein the abscissa is the multiple of the unit distance, the ordinate is the value of $dRMS^2_R(P^*, Q^*)$, and the legend is the rotation angle.

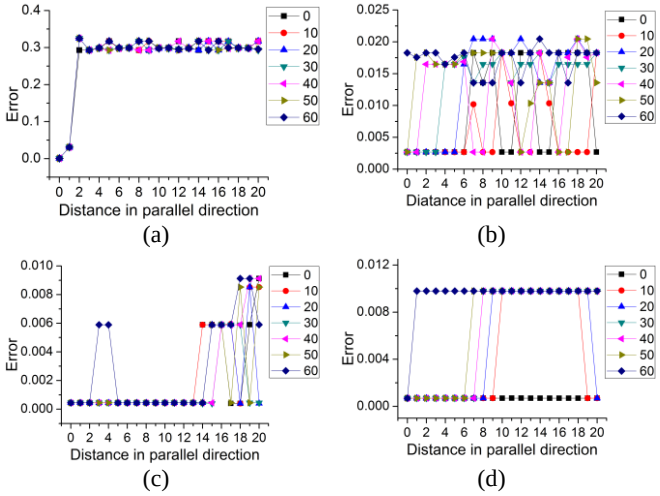

FIGURE 22. Registration errors with the rotation angle-distance along the parallel direction: (a) Armadillo, (b) Duck, (c) Mario, and (d) Chef.

In the parallel direction, the registration results of the Duck and the Chef are similar, that is, the effective distance gradually decreases as the rotation angle increases. When the rotation angle is between 0-60 degrees (a local optimum is trapped when the rotation angle is above 60 degrees and the distance exceeds 0 times), the effective distance multiples of the Duck are 6, 6, 5, 3, 1, and 0, and the Chef datasets are 20, 9, 8, 7, 7, 6, and 1. For the Armadillo datasets, the effective horizontal distances are still the smallest, and all are trapped at a local optimum when the distance exceeds 1 time. The Mario maintains the breadth and stability of the previous section, and its effective distance is roughly stable at 13-15 times. As mentioned earlier, the most common cause of this difference is the shape of the point set object. The horizontal profile of the Armadillo resembles a horseshoe shape, which makes it more sensitive to the distance and rotation angle, while the other three shapes are more singular. In addition, the Mario possesses more outliers and scattered points, and this makes the ICP-based registration result robust because these scattered points have a point-to-point correspondence with different points. The Duck and the Chef datasets are somewhere in between.

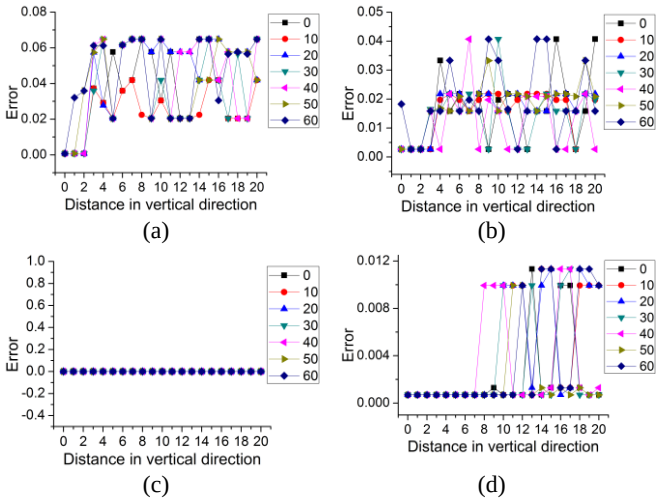

FIGURE 23. Registration errors with the rotation angle-distance along the vertical direction: (a) Armadillo, (b) Duck, (c) Mario, and (d) Chef.

In the vertical direction, the results of the registration are similar to those based on the sampling angle-distance. The effective distances of the Armadillo are 1-4 times, which represents an increase over the parallel direction. Those of the Duck are instead reduced, and the results are 0-4 times. When the sampling angle is 30 degrees, the effective distances of the Mario are the largest, which are all 20 times, and those of the Chef remain at the intermediate level. Outside the effective distance, the up and down swing frequency and the swing amplitude of $dRMS^2_R(P^*, Q^*)$ in the vertical direction are higher than those in the horizontal direction, which indicates that the registration stability in the vertical direction is worse than that in the horizontal direction.

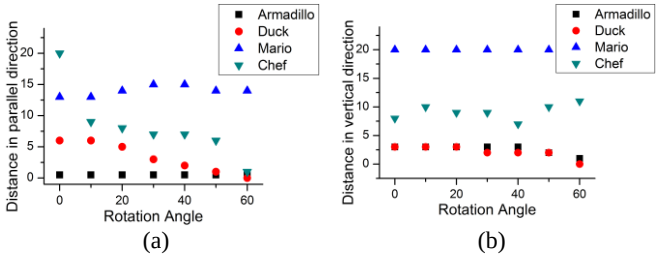

FIGURE 24. Effective critical point of each dataset based on the rotation angle-distance: (a) Parallel direction and (b) vertical direction.

Figure 24 shows the effective ranges of the four datasets based on the rotation angle-translation multiple in both directions. It can be seen that in the parallel direction, as the rotation angle increases, the effective distance mostly declines, and even some datasets (the Chef and the Duck) appear to decrease rapidly. At the same time, the effective distances of the Armadillo, the Duck and the Chef datasets tend to be 0 times the unit distance at a rotation angle of 60 degrees. This shows that the rotation angle and distance both have an effect on the effectiveness of the ICP algorithm. The general upper limit of the rotation angle is 60 degrees, and the horizontal and vertical directions are 0.5 times and 1 times the unit distance.

This article has been accepted for publication in a future issue of this journal, but has not been fully edited. Content may change prior to final publication. Citation information: DOI 10.1109/ACCESS.2020.2986470, IEEE Access

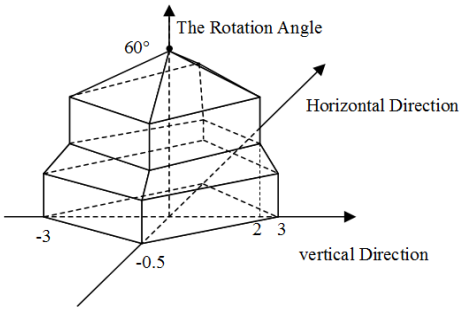

FIGURE 25. Universal effective range fitting based on the rotation angle-distance.

Figure 25 is a general effective range fitting result based on the rotation angle-distance, and the three-dimensional interior is the effective range. It should be noted that since the effective distance threshold in the horizontal direction is 0 times the unit distance (Figure 24b), when the rotation angle is increased to 30 degrees in Figure 25, the threshold in the horizontal direction is scaled down by the relative change in the vertical direction; the scale down is two-thirds the size of 0.5 times the unit distance.

B. VALIDITY OF POINT-TO-PLANE ICP

In this section, the point-to-plane ICP algorithm is used to perform the same experiments as in Section 4.1. The experimental results no longer give the error of each ICP as in Section 4.1 but only compare each effective range with that of point-to-point ICP.

1) VALIDITY BASED ON SAMPLING ANGLE - ROTATION ANGLE

Figure 26 shows the effective thresholds of the sampling angle-rotation angle for the point-to-point and point-to-plane ICP algorithms under four datasets. In the Armadillo datasets, when the sampling angle is 30 degrees, the two ICP algorithms have the same effective threshold of rotation angle. In addition, the effective threshold of point-to-plane ICP is 10 degrees smaller than that of point-to-point ICP. In the Duck datasets, the effective ranges of point-to-plane ICP are greater than those of point-to-point ICP when the sampling angles are 20 and 40 degrees, while the ranges are less than those of the point-to-point in other cases. The results of the Mary datasets are similar to those of the Duck datasets. The only difference is that the effective range of the two ICP algorithms is the same when the sampling angles are 20 and 40 degrees. In the Chef datasets, there are two effective thresholds for the rotation angle of point-to-plane ICP that are greater than those of the point-to-point, which is when the sampling angles are 0 and 20. Meanwhile, when the sampling angle is 80 degrees the two ICPs are the same, and in the other cases point-to-point ICP has advantages.

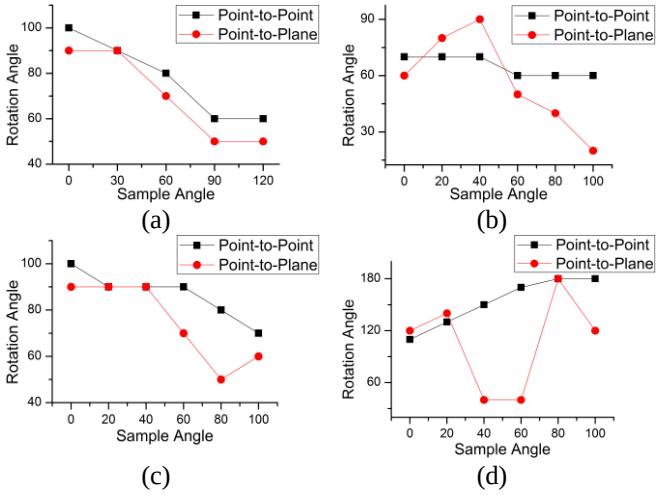

FIGURE 26. Comparison of the effective ranges based on the sampling angle-rotation angle: (a) Armadillo, (b) Duck, (c) Mario, and (d) Chef.

From the commonness of the four datasets, the effective range of the point-to-plane ICP algorithm is superior to that of the point-to-point only at a sampling angle of 20 degrees, and the rest are smaller. Figure 27 shows the results of extracting the minimum effective thresholds of the two ICP algorithms and performing linear fittings. It can be seen from the figure that the fitting line of point-to-plane ICP is lower than that of the point-to-point, which indicates that the effective range of the point-to-plane ICP algorithm based on the sampling angle-rotation angle is generally inferior to that of the point-to-point.

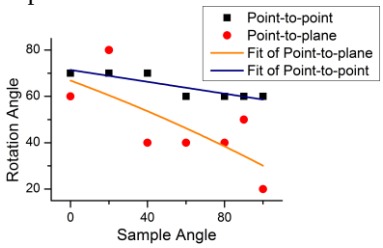

FIGURE 27. Comparison of the general effective range fittings between point-to-point and point-to-plane ICPs based on the sample angle-rotation angle.

2) VALIDITY BASED ON SAMPLING ANGLE - DISTANCE

Figure 28 shows the effective thresholds of the two ICP algorithms based on the sampling angle-horizontal distances for the four datasets. In all results, only when the sampling angle of the Armadillo datasets is 30 degrees (Figure 28a) is the effective horizontal distance of point-to-plane ICP greater than that of point-to-point ICP. Concurrently, when the sampling angles of the Armadillo datasets are more than 60 degrees, the effective distances of the two algorithms are the same. In other cases, the effective horizontal distance of point-to-plane ICP is better than that of the point-to-point. Furthermore, most effective horizontal distances are within 0.5 times the distance. This shows that the point-to-plane ICP algorithm has a smaller effective horizontal distance for different sampling angles.

This article has been accepted for publication in a future issue of this journal, but has not been fully edited. Content may change prior to final publication. Citation information: DOI 10.1109/ACCESS.2020.2986470, IEEE Access

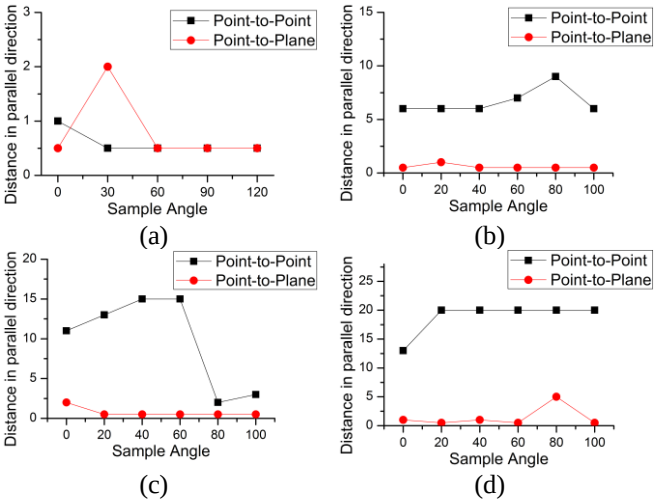

FIGURE 28. Comparison of the effective ranges based on the sampling angle-distance along the parallel direction: (a) Armadillo, (b) Duck, (c) Mario, and (d) Chef.

Figure 29 is a comparison of the effective thresholds based on the sampling angle-vertical distance. The point-to-plane ICP algorithm is better than the point-to-point ICP algorithm overall in the results from the Chef datasets and is worse in those from the other datasets. From the minimum thresholds of the four datasets, the point-to-plane ICP is also worse than the point-to-point ICP, and its effective ranges are all within 0.5 times the unit distance.

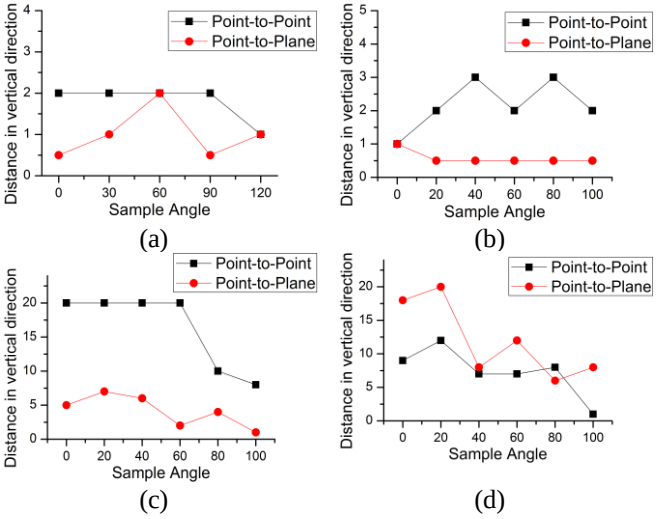

FIGURE 29. Comparison of the effective ranges based on the sampling angle-distance along the vertical direction: (a) Armadillo, (b) Duck, (c) Mario, and (d) Chef.

Figure 30 shows the results of extracting the minimum effective distance of the two ICP algorithms and performing linear fitting, where Figure a is the comparison in the horizontal direction and b is the comparison in the vertical. Except when the sampling angle is 30 degrees, the minimum distance thresholds of point-to-plane ICP in the horizontal direction are all within 0.5 times the unit distance, which is less than those of point-to-point ICP. The results in the vertical direction are also similar. This indicates that the effective distance of point-to-plane ICP at different sampling angles is less than that of point-to-point ICP.

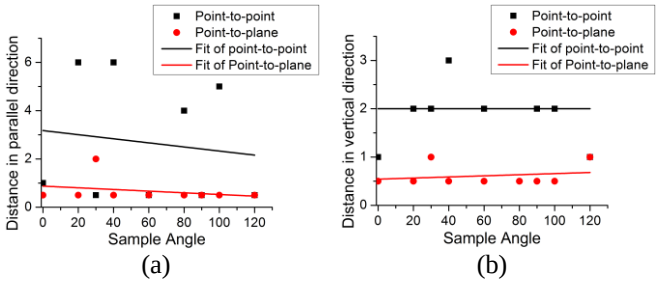

FIGURE 30. Comparison of the universal effective distances between point-to-point and point-to-plane ICPs based on the sampling angle-distance: (a) Parallel direction and (b) vertical direction.

3) VALIDITY BASED ON ROTATION ANGLE - DISTANCE

Figure 31 shows the effective thresholds of the two ICP algorithms based on the rotation angle-horizontal distances for the four datasets. In the four datasets, the horizontal effective distance thresholds of point-to-plane ICP in the Armadillo datasets are all greater than those in point-to-point ICP. In addition, the result of point-to-plane ICP in the Chef datasets with a rotation angle of 20 degrees is also better. In all other results, the point-to-plane ICP results are worse than those of the point-to-point.

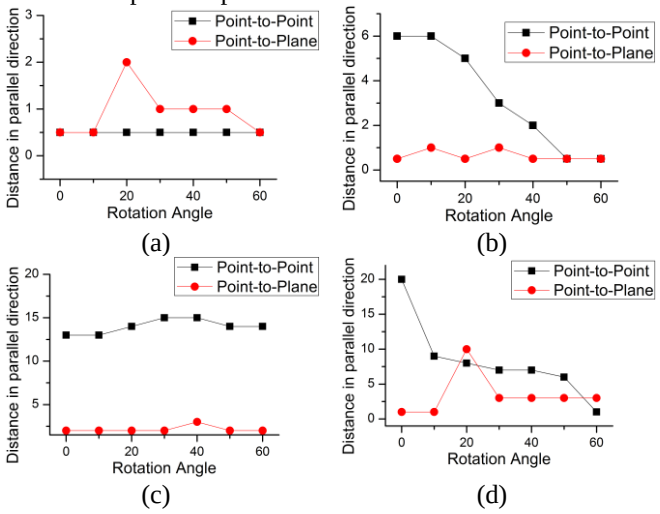

FIGURE 31. Comparison of the effective ranges based on the rotation angle-distance along the parallel direction: (a) Armadillo, (b) Duck, (c) Mario, and (d) Chef.

Figure 32 is the comparison of the effective thresholds based on the rotation angle-vertical distance. The thresholds of point-to-plane ICP for vertical effective distance in the Armadillo, Duck, and Mary datasets are all worse than point-to-point ICP. Only when the rotation angle of the Che datasets is less than 20 degrees, the point-to-plane is better.

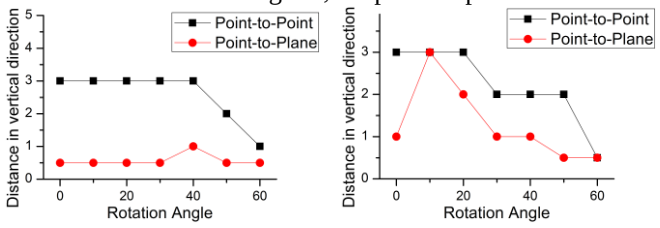

This article has been accepted for publication in a future issue of this journal, but has not been fully edited. Content may change prior to final publication. Citation information: DOI 10.1109/ACCESS.2020.2986470, IEEE Access

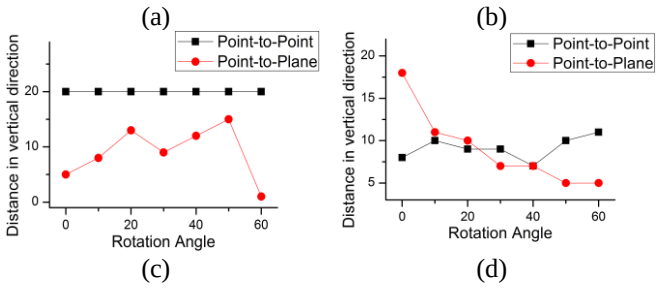

FIGURE 32. Comparison of the effective ranges based on the rotation angle-distance along the vertical direction: (a) Armadillo, (b) Duck, (c) Mario, and (d) Chef.

Similarly, the smallest thresholds in the four datasets are extracted to form the smallest distance ranges, and a linear fit is performed to obtain a universal range based on the rotation angle-vertical distance. Figure 33 provides comparisons of the general ranges between the two ICP algorithms in the parallel and vertical directions.

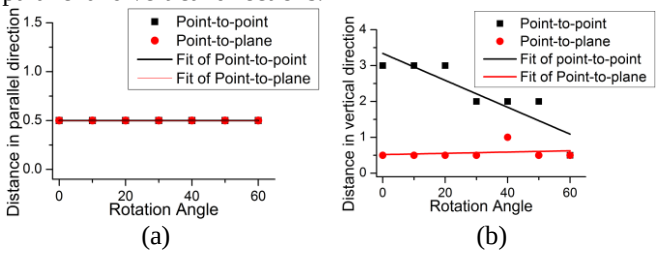

FIGURE 33. Comparison of the universal effective distances between point-to-point and point-to-plane ICPs based on the rotation angle-distance: (a) Parallel direction and (b) vertical direction.

The universal effective distances of the two ICP algorithms is the same in the parallel direction, while in the vertical direction, point-to-point ICP is better than point-to-plane ICP.

In general, from the effective range of sampling angles, rotation angles and distances, the point-to-point ICP algorithm is better than point-to-plane ICP.

C. ROBUSTNESS OF ICP

To verify the effect of Gaussian noise on the validity of the ICP algorithm, the Armadillo datasets with five levels of Gaussian noise are implemented with the two ICP algorithms. Figures 34 and 35 show the results of two ICPs with noiseless datasets and five levels of Gaussian noise datasets at different sampling and rotation angles in Armadillo. In the legend, "non" indicates clean datasets, and the numbers indicate the level of Gaussian noise (see Section 3.2.4 for details). Figures a, b, c, and d are the results of sampling angles of 0, 30, 60, and 90 degrees, respectively.

From Figure 13a, we know that the effective rotation angles of point-to-point ICP with the Armadillo datasets at sampling angles of 0, 30, 60, and 90 degrees are 100, 90, 80, and 60 degrees, respectively. By comparison, in Figure 34, it can be found that the results of the five levels of Gaussian noise datasets are basically consistent with those of the noiseless datasets, that is, their effective thresholds are the same. Unlike the non-noise datasets, the *dRMS*(error) of the Gaussian noise datasets are significantly higher when the ICPs fall into a local optimum.

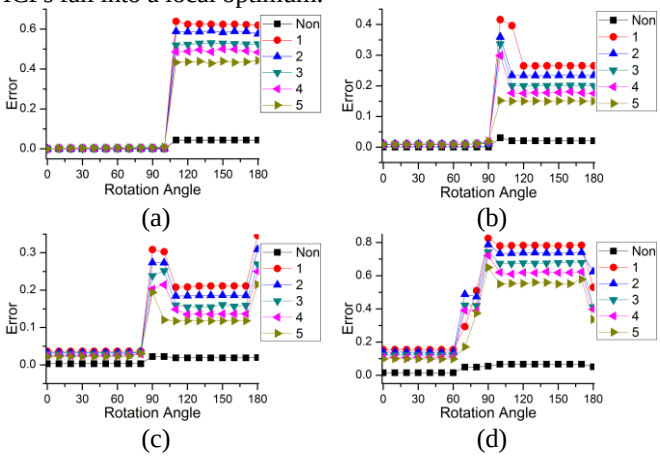

FIGURE 34. Registration errors of point-to-point ICP with Gaussian noise at different levels: (a) 0-degree sampling angle, (b) 30-degree sampling angle, (c) 60-degree sampling angle, and (d) 90-degree sampling angle.

In the valid range of the rotation angles, the errors of the five levels of the Gaussian noise datasets are almost the same as those of the noiseless datasets when the sampling angle is 0 degrees. As the sampling angle increases, the gap becomes larger. As the Gaussian noise level increases, the error decreases. This is because ICP excludes points whose distance exceeds the threshold when calculating the error.

In addition, it should be noted that, not only in the other three types of data (Duck, Mario and Chef) but also based on the sampling angle-distance and rotation angle-distance, the effective ranges of point-to-point ICP with the five levels of the Gaussian noise datasets are completely consistent with those of the non-noise datasets. The difference is that the errors are diverse when ICP is trapped in a local optimum. These are no longer explained in this paper.

However, the results of point-to-plane ICP (Figure 35) with the Gaussian noise datasets are different from those of point-to-point ICP. When the sampling angle is 0 degrees, the effective rotation angle with no noise is 90 degrees. However, the valid values for Gaussian noise from levels 1 to 5 are 100, 110, 80, 110, and 100. Except for the level-3 Gaussian noise, the effective rotation angle of other Gaussian noise datasets is actually larger than that of the noiseless data, and this situation is similar for other sampling angles. The reason may be that point-to-point ICP only relies on independent points to establish correspondence, and noise points can be filtered by the least squares method. In the point-to-plane ICP algorithm, the normal of a point, which is determined by the neighbor points, will be affected by noise points.

This article has been accepted for publication in a future issue of this journal, but has not been fully edited. Content may change prior to final publication. Citation information: DOI 10.1109/ACCESS.2020.2986470, IEEE Access

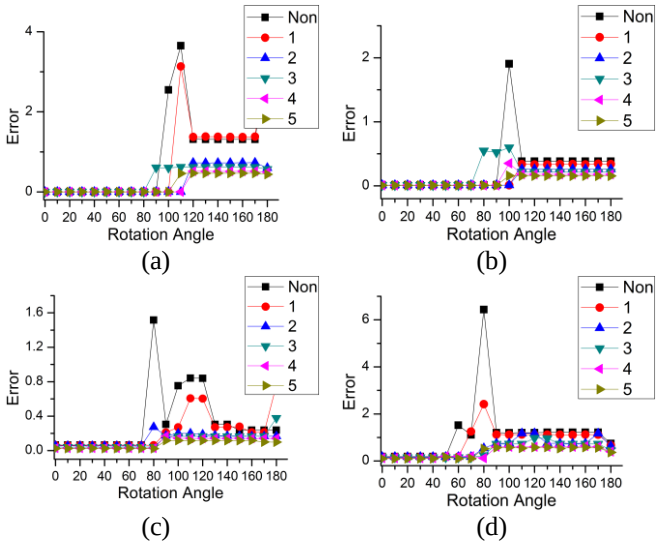

FIGURE 35. Registration errors of point-to-plane ICP with Gaussian noise at different levels: (a) 0-degree sampling angle, (b) 30-degree sampling angle, (c) 60-degree sampling angle, and (d) 90-degree sampling angle.

On the other hand, by comparing the errors in Figs. 34 and 35, it can be found that the point-to-plane ICP of no-noise and Gaussian-noise within the effective range has almost the same error, while the error of point-to-point ICP with Gaussian noise increases with the sampling angle. This shows that point-to-plane ICP is more robust to Gaussian noise than point-to-point ICP is in terms of accuracy.

Overall, the point-to-point ICP algorithm is robust to Gaussian noise with respect to validity, and the smaller the sampling angle is, the stronger the ICP anti-noise capability. The point-to-plane ICP is more resistant to Gaussian noise in terms of accuracy.

D. ACCURACY OF ICP

The ICP algorithm may fall into a local optimum, so the registration result will be correct or wrong. In this section, the registration accuracy of ICP only under the correct results are analyzed. The $dRMS^2_R(P^*, Q^*)$ value can reflect the accuracy of the registration result to some extent. From Figs. 22 and 23, if the two datasets used for registration are the same, as long as the ICP results are correct, the $dRMS^2_R(P^*, Q^*)$ values must be the same regardless of the angle and distance. This shows that the rotation angle and distance have no effect on the accuracy of the ICP registration under the correct registration. From Figs. 13, 16 and 19, when the sampling angle is different, the values under the correct result are different. Therefore, it can be said that the sampling angle has a direct impact on the accuracy of the registration. This section focuses on errors at different sampling angles.

Figure 36a shows the $dRMS^2_R(P^*, Q^*)$ values of ICP at different sampling angles within the effective range of the four datasets. From the figure, the relative error does not increase strictly with the sampling angle but decreases with certain thresholds. For example, when the sampling angle of the Duck is 40, the Mario is 100, and the Chef 60, the relative errors begin to decrease. This is because $dRMS^2_R(P^*, Q^*)$ is mainly used to describe the average error of the nearest neighbors in the two datasets. However, the nearest neighbor often does not necessarily have a point-to-point correspondence. When the sampling angle of the two points is larger (a smaller the overlap ratio), the more likely a nonidentical point is.

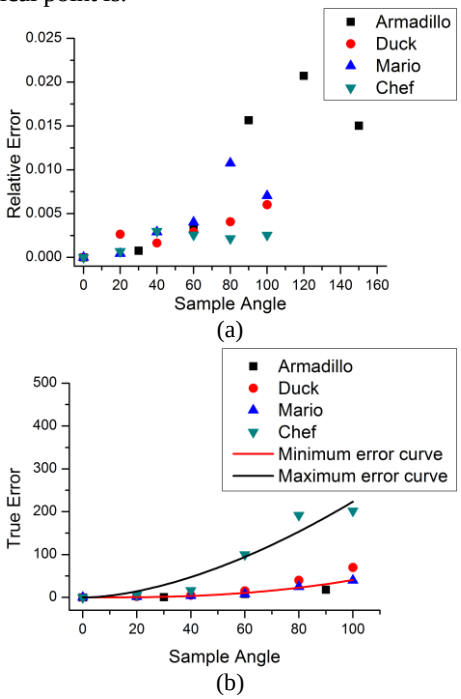

FIGURE 36. Two kinds of registration accuracies: (a) $dRMS^2_R$ and (b) true error.

To correctly describe the true registration accuracy of the ICP algorithm, the source datasets are superimposed with the target datasets, and the ratio of the average error to the nearest neighbor distance is calculated by manually selecting the point-to-point correspondence, which is used as the real error. Figure 36b shows the true error for the different sampling angles of the four datasets. Very different from the relative error, the true error of the Chef is the largest. The other three datasets have similar errors when the sampling angle is less than 60 degrees, while having certain differences beyond 60 degrees. The reason is shown in Figure 12. The horizontal points of the Chef datasets are close to the arc, which is more likely to cause misalignment errors in the figure.

The black and red dashed lines in Figure 36b are the fitted lines of the maximum and minimum errors, which all conform to the regularity of the quadratic curve. When the sampling angle is 20 degrees, the true values of the Chef is 5 times the nearest neighbor distance, and the other three datasets are maintained at 2 times. When the sampling angle is 40 degrees, the Chef is approximately 15 times, while the other datasets are within 5. When the sampling angle is increased to 60 degrees, the Chef and others are respectively 100 and 10 times. This observation shows that as the

This article has been accepted for publication in a future issue of this journal, but has not been fully edited. Content may change prior to final publication. Citation information: DOI 10.1109/ACCESS.2020.2986470, IEEE Access

sampling angle increases, the error increases rapidly. In terms of applicability, if a higher registration accuracy is to be achieved, of course, the smaller the sampling angle is, the better. When the horizontal section of the point cloud dataset is similar to an arc, the reasonable sampling angle is within 20 degrees, or no more than 30 degrees, which is less than the 40 degrees of the other datasets.

E. EFFICIENCY OF ICP

The efficiency analysis in this section is based on the relative run time and the number of iterations (Section 3.4.3). Figure 37 shows the relative run time of the ICP algorithm under different conditions, where a is the relative run time at different rotation angles when the minimum sampling angle is the minimum value greater than 0 degrees (the composite data is 30 degrees, and the remaining point clouds are 20 degrees), and the distance is 0 times in the four datasets; b is based on the sampling angle - the rotation angle of the Armadillo datasets (the legend is the sampling angle); and c and d are in the two directions of parallel and vertical with datasets that are the same as those in a.

In Figure 37a, the relative run time for the four datasets increases slowly with the rotation angle, which indicates that the rotation angle has a certain influence on the efficiency of ICP. Meanwhile when the growth time reaches a certain angle, the relative run time has a sudden increase. In the four datasets, the Armadillo datasets have a sudden rotation angle of 100 degrees, the Duck of 80 degrees, the Mario of 100 degrees, and the Chef of 140 degrees. It can be found from the orange line segment in Figure 13 that these four rotation angles are exactly the validity thresholds of the respective datasets. This shows that the effective threshold can also be obtained by observing the trend of the relative run time of ICP.

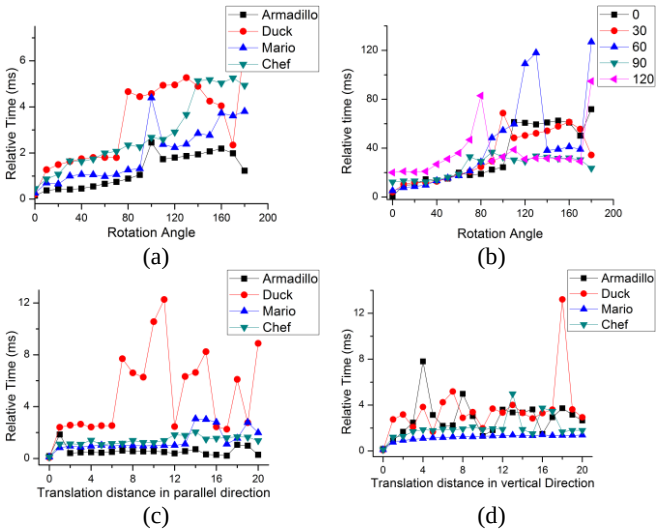

FIGURE 37. Comparison of ICP algorithm efficiencies for different parameters: (a) Relative time of four datasets based on the rotation angle, (b) relative time of the Armadillo datasets based on the sampling angle-rotation angle, (c) relative time of the four dataset types based on the parallel distance, and (d) relative time of the four dataset types based on the vertical distance.

For the Armadillo datasets in Figure 37b, the rotation angles when the run time is abrupt are 100, 90, 80, 60, and 70 for a sampling angle of 0-120 degrees. Compared with Figure 13a, except for the sampling angle of 120 degrees, the results of the other sampling angles are completely consistent. This result also verifies the previous theory that when the ICP falls into a local optimum, the run time of the algorithm will be abrupt. In addition, by comparing the mutation points with their previous points at different sampling angles, the difference gradually decreases as the sampling angle increases. The reason is that the error is becoming larger, which is described in Section 4.4. Except for the 120-degree sampling angle, the curves of the relative run time are almost identical within their effective range. From Figure 37b, the relative errors of the registration results with a sampling angle of 120 degrees in the Armadillo datasets exceed 100 times the unit distance, so it can be excluded. Therefore, it can be concluded that the sampling angle hardly affects the efficiency of the registration within the effective range of ICP.

In Figures c and d, the angle thresholds of the abrupt points are consistent with the critical values of the effective range of the distance (except 0 times the distance) in both directions. At the same time, the stability in the horizontal direction is slightly better than that in the vertical direction. However, the Armadillo datasets are an exception, probably because of the shape as discussed before. Except 0 times the unit distance, the relative run time within the effective range is relatively stable. This shows that the effect of distance on the efficiency of ICP mainly reflects whether the two datasets overlap. Two overlapping datasets have a better registration efficiency than do separated ones. However, once the positions of the two datasets do not coincide, the distance also has little effect on the efficiency of ICP no matter how far apart they are.

The number of iterations is used to analyze the efficiency of point-to-point and point-to-plane ICPs. It can be seen from Figure 37 that the rotation angle has an important influence on the ICP efficiency, and the sampling angle and distance have a limited effect on it. Therefore, the efficiency comparison of point-to-point and point-to-plane ICPs only considers the difference in rotation angles.

Figure 38 shows the comparison of the number of iterations between the two ICP algorithms at different rotation angles within the effective range when the sampling angles are 0, 30, and 60 degrees. It can be seen from the figure that the number of iterations of both ICP algorithms increases simultaneously with the rotation angle. However, the increase in the number of iterations is different between the two types of ICP. The point-to-plane ICP algorithm has fewer iterations than does point-to-point ICP under the same conditions. Except for the 0-degree rotation angle, the minimum number of iterations for point-to-point ICP is more than 10, and the maximum is close to 40. The number for point-to-plane ICP is only between 3-15, and most of them are less than 10. In addition, the sampling angle hardly affects the efficiency of point-to-plane ICP for a 60-degree

This article has been accepted for publication in a future issue of this journal, but has not been fully edited. Content may change prior to final publication. Citation information: DOI 10.1109/ACCESS.2020.2986470, IEEE Access

sampling angle. For point-to-point ICP, the efficiencies at the sampling angles of 0 degrees and 30 degrees are almost the same, but when the sampling angle is 60 degrees, the efficiency is improved. Therefore, the efficiency of point-to-plane ICP is better than that of point-to-point ICP, but as the sampling angle increases, the advantage of point-to-plane ICP decreases.

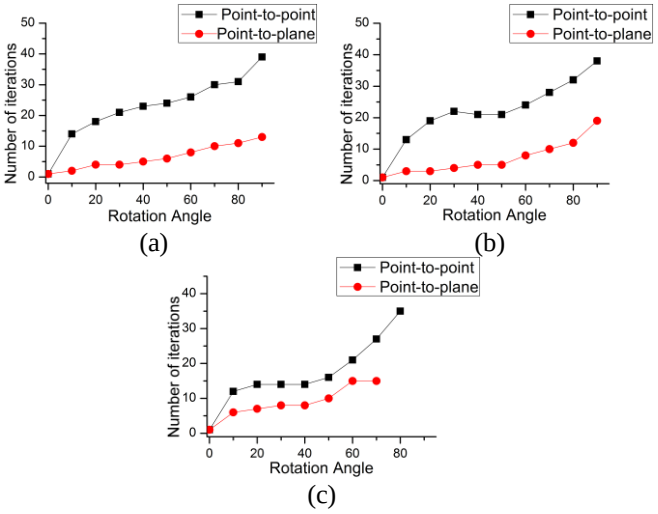

FIGURE 38. Comparison of iterations between the two ICP algorithms: (a) 0-degree sample angle, (b) 30-degree sample angle, and (c) 60-degree sample angle.

In conclusion, the rotation angle has an important effect on the efficiency of the ICP algorithm, and the number of iterations increases with it. The effects of sampling angle and distance on efficiency are limited. Point-to-plane ICP is more efficient than point-to-point ICP.

V. DISCUSSION

The ICP algorithm presents effective thresholds for the rotation angle and distance. Once the threshold is exceeded, ICP is likely to fall into a local optimal solution. Under the premise that the center points of the two datasets are close, the minimum effective rotation angle of point-to-point ICP is 60 degrees. Point-to-plane ICP has a smaller effective rotation angle, which is 40 degrees when the sampling angle is less than 80 degrees. Similarly, the effective distance of point-to-point ICP is greater than that of point-to-plane ICP. The effective distance of the former is between 0.5 and 6 times the unit distance (depending on the difference in the sampling angle and rotation angle), while that of the latter is mostly within 0.5 times. It should be noted that Figs. 27, 30, and 33 show the effective ranges of each of the two parameters, which are established on the premise that the third parameter is optimal. If the third parameter is not optimal, the effective range of the first two parameters will be further reduced. To ensure reliability, the effective distance of both ICP algorithms is best kept within 0.5 times the unit distance.

In terms of robustness, the effect of Gaussian noise on the validity of point-to-point ICP is negligible, but it does increase the result error of point-to-point ICP. In contrast, the validity of point-to-plane ICP is affected by Gaussian noise, but in most cases, the effective range is only increased slightly. The accuracy of point-to-plane ICP is less affected by Gaussian noise. Therefore, point-to-point ICP is more robust with respect to effectiveness, while point-to-plane ICP is more resistant to Gaussian noise in terms of accuracy.

The accuracy of ICP is only determined by the sampling angle of the two datasets, regardless of the rotation angle and distance. As the sampling angle increases, the error increases exponentially. Therefore, to ensure the accuracy of registration, the reasonable sampling angle of the two datasets used for registration should be between 20 and 30 degrees.

The rotation angle has a direct impact on the efficiency of the two ICP algorithms, and the larger the angle is, the more iterations required. Distance has a certain effect on efficiency, but when the distance exceeds one times the unit distance, the efficiency is similar, regardless of the distance. The effect of sampling angle on efficiency is small. In addition, the efficiency of the point-to-plane ICP algorithm is better than that of point-to-point under the same conditions.

For both ICP algorithms, the validity of point-to-point ICP is wider and more robust than that of point-to-plane ICP. However, the latter undergoes fewer iterations, and its accuracy is more robust to Gaussian noise. This paper does not evaluate point-to-line ICP, but in theory, it should be between point-to-point and point-to-plane ICPs in terms of effective range, robustness and efficiency.

It can be known that when the two datasets need to be registered, we only need to know the parameters of the sampling angle, rotation angle, and distance to determine whether the initial position is within the valid range and whether coarse registration needs to be performed before ICP registration. The sampling angle is determined at the time of data collection, which only needs to be set according to the optimal range given in this paper. Because point cloud scans are leveled when collecting point cloud datasets, the approximate plane of an object perpendicular to the horizontal plane can be estimated. The angle between the approximate planes of the two datasets is the rotation angle, and the only thing that needs to be considered is the direction. Additionally, the distance can be determined by the location of the center of the two datasets.

Once the rotation angle and distance are known, coarse registration will become faster, if it is required. Because the scanning device is level, coarse registration no longer requires three rotation angles along the three axes, but only one along an axis perpendicular to the horizontal plane. This angle is exactly similar to the rotation angle mentioned above. The difference between the two center points in the three axis directions is the translation. The rigid transformation matrix can be quickly constructed from a rotation angle along an axis perpendicular to the horizontal plane and from translations in three directions. This is our future work.

This article has been accepted for publication in a future issue of this journal, but has not been fully edited. Content may change prior to final publication. Citation information: DOI 10.1109/ACCESS.2020.2986470, IEEE Access

VI. CONCLUSION

In this study, the ICP algorithms in point cloud registration are evaluated. Four types of point cloud datasets are taken as the research object, and the effective thresholds of the two ICP algorithms in overlap rate, rotation angle and distance are discussed. The minimum critical values of the four datasets are selected, and the general effective ranges of ICP for the three parameters are determined. In addition, the accuracy variation law of the ICP algorithm and the factors affecting the accuracy are analyzed in the effective ranges. The influencing factors and their changing rules of efficiency are analyzed based on ICP run time, and the efficiency of two ICPs is compared based on the number of iterations.

REFERENCES

[1] P. J. Besl, and H. D. McKay, "A method for registration of 3-D shapes," *IEEE Transactions on Pattern Analysis and Machine Intelligence*, vol. 14, no. 2, pp. 239-256, Feb. 1992.

[2] R. B. Rusu, "Semantic 3D Object Maps for Everyday Manipulation in Human Living Environments," Ph.D. dissertation, Künstliche Intelligenz, Technischen Universität München, Germany, 2010.

[3] N. Gelfand et al., "Geometrically Stable Sampling for the ICP Algorithm," in *Proceedings of the Fourth International Conference on 3-D Digital Imaging and Modeling*, Banff, Alberta, Canada, 2003.

[4] R. Benjemaa, and F. Schmitt, "Fast global registration of 3D sampled surfaces using a multiz-buffer technique," *Image and Vision Computing*, vol. 17, no. 2, pp. 113-123, Apr. 1999.

[5] J. Zhu, C. Jin, Z. Jiang, et al., "Robust point cloud registration based on both hard and soft assignments," *Optics and Laser Technology*, vol. 110, pp. 202-208, Feb. 2019.

[6] J. Zhu, Z. Jiang, G. D. Evangelidis, et al., "Efficient registration of multi-view point sets by K-means clustering," *Information Sciences*, vol. 488, pp. 205-218, Jul. 2019.

[7] J. Han, P. Yin, Y. He, and F. Gu, "Enhanced ICP for the Registration of Large-Scale 3D Environment Models: An Experimental Study," *SENSORS*, vol. 16, no. 2, pp. 228-242, Feb. 2016.

[8] G. Turk, and M. Levoy, "Zippered polygon meshes from range images," in *Proceedings of SIGGRAPH 94 21st International ACM Conference on Computer Graphics and Interactive Techniques*, SIGGRAPH 1994 ACM, Orlando, FL, USA, 1994.

[9] T. Masuda, K. Sakaue, and N. Yokoya, "Registration and Integration of Multiple Range Images for 3-D Model Construction," in *Proceedings of International Conference on Pattern Recognition IEEE*, Vienna, Austria, 1996.

[10] A. D. Sappa, M. Devy, and A. Restrepo-Specht, "Range Image Registration by using an Edge-Based Representation," In *Proceedings of the 9th International Symposium on Intelligent Robotic Systems*, Toulouse, France, 2001, pp. 167-176.

[11] Z. Zhang, "Iterative Point matching for registration of freeform curves and surfaces," *International Journal of Computer Vision*, vol. 13, no. 2, pp. 119-152, Apr. 199.

[12] M. Greenspan, and M. Yurick, "Approximate K-D Tree Search for Efficient ICP," in *Proceedings of the Fourth International Conference on 3-D Digital Imaging and Modeling*, Banff, Alberta, Canada, 2003.

[13] A. Censi, "An ICP variant using a point-to-line metric," in *Proceedings of IEEE International Conference on Robotics and Automation*. Pasadena, California, USA, 2008.

[14] D. Grant, J. Bethel, and M. Crawford, "Point-to-plane registration of terrestrial laser scans," *ISPRS Journal of Photogrammetry and Remote Sensing*, vol. 72, no. none, pp. 181-186, Aug. 2012.

[15] Y. Chen, and G. Medioni, "Object modelling by registration of multiple range images," in *Proceedings of 1991 IEEE International Conference on Robotics and Automation*, Sacramento, California, USA, 1991.

[16] Y. Shen, L. Hu, and B. Li, "Morbidity Problems and Solutions of Bursa Model for Local Region Coordinate Transformation," *Acta Geodaetica et Cartographica Sinica*. vol. 35, no. 1, pp. 95-98, Jan. 2006.

[17] H. Wolf, "Scale and orientation in combined Doppler and triangulation nets," *J GEODESY*., vol. 54, no. 1, pp. 45-53, Jan. 1980.

[18] T. Soler, "A compendium of transformation formulas useful in GPS work," *J GEODESY*., vol. 72, no. 7, pp. 482-490, Aug. 1998.

[19] B. Schaffrin, I. Lee, Y. Felus, and Y. Choi, "Total least-squares (TLS) for geodetic straight-line and plane adjustment," *Bollettino Di Geodesia E Scienze Affini*, vol. 65, no. 3, pp. 141-168, Sep. 2006.

[20] B. Schaffrin, "A note on constrained total least-squares estimation," *LINEAR ALGEBRA APPL*., vol. 417, no. 1, pp. 245-258, Aug. 2006.

[21] B. Schaffrin, and Y. A. Felus, "An algorithmic approach to the total least-squares problem with linear and quadratic constraints," *STUDIA GEOPHYSICA ET GEODAETICA*, vol. 53, no. 1, pp. 1-16, Jan. 2009.

[22] J. Lu, Y. Chen, B. F. Li, and X. Fang, "Robust Total Least Squares with reweighting iteration for three-dimensional similarity transformation," *SURV REV*., vol. 46, no. 334, pp. 28-36, Jan. 2014.

[23] Y. Q. Tao, J. X. Gao, and Y. F. Yao, "TLS algorithm for GPS height fitting based on robust estimation," *SURV REV*., vol. 46, no. 336, pp. 184-188, May. 2014.

[24] M. S. Foster, J. R. Schott, and D. W. Messinger, "Spin-image target detection algorithm applied to low density 3D point clouds," *Journal of Applied Remote Sensing*, vol. 2, no. 1, pp. 023539, Jan. 2008.

[25] A. Frome, D. Huber, R. Kolluri, T. Bülow, and J. Malik, (2004). "Recognizing objects in range data using regional point descriptors," In *Proceedings of the 8th European Conference on Computer Vision*, Prague, Czech, 2004, pp. 224-237.

[26] F. Tombari, S. Salti, and L. Stefano, "Unique signatures of histograms for local surface description," In *Proceedings of 11th European Conference on Computer Vision*, Springer, New York, USA. 2010, pp. 356–369.

[27] S. Salti, F. Tombari, and D. Stefano, (2014). "SHOT: Unique signatures of histograms for surface and texture description," *Computer Vision and Image Understanding*, vol. 125, no. 8, pp. 251-264, Aug. 2014.

[28] F. Tombari, S. Salti, and L. Stefano, (2010a), "Unique shape context for 3D data description," In *Proceedings of the ACM workshop on 3D object retrieval*, Firenze, Italy, 2010, pp. 57-62.

[29] R. B. Rusu, N. Blodow, Z. C. Marton, and M. Beetz, "Aligning point cloud views using persistent feature histograms," In *Proceedings of 2008 IEEE/RSJ International Conference on Intelligent Robots and Systems*, Nice, France, 2008, pp.3384–3391.

[30] R. B. Rusu, N. Blodow, and M. Beetz, "Fast point feature histograms (FPFH) for 3D registration," In *Proceeding of 2009 IEEE International Conference on Robotics and Automation*, Kobe, Japan, 2009, pp. 3212–3217.

[31] Y. Guo, M. Bennamoun, F. Sohel, J. Wan, and M. Lu, "3D free form object recognition using rotational projection statistics," In *Proceedings of IEEE 14th Workshop on the Applications of Computer Vision*, Tampa, FL, USA, 2013, pp. 1-8.

[32] H. Chen, and B. Bhanu, "3Dfree-form object recognition in range images using local surface patches," *Pattern Recognition Letters*, vol. 28, no. 10, pp. 1252-1262, Oct. 2007.

[33] Y. Guo, F. Sohel, M.Bennamoun, J. Wan, and M. Lu, "A novel local surface feature for 3D object recognition under clutter and occlusion," *Information Sciences*, vol. 293, no. 2, pp. 196-213, Apr. 2015.

[34] C. Chen, Y. Hung, and J. Cheng, "RANSAC-based DARCES: A new approach to fast automatic registration of partially overlapping range images," *IEEE Transactions on Pattern Analysis and Machine Intelligence*, vol. 21, no. 11, pp. 1229-1234, Nov. 1999.

[35] N. Gelfand, N. J. Mitra, L. J. Guibas, and P. Helmut, "Robust global registration," In *Symposium on Geometry Processing*, Vienna, Austria, 2005.

[36] D. Aiger, N. J. Mitra, and D. Cohen-Or, "4-points congruent sets for robust pairwise surface registration," *ACM Transactions on Graphics*, vol. 27, no. 3, pp. 85-94, Aug. 2008.

[37] P. Li, J. Wang, Y. D. Zhao, Y. X Wang, and Y. F. Yao. "Improved algorithm for point cloud registration based on fast point feature

histograms," *Journal of Applied Remote Sensing*, vol. 10, no. 4, pp. 045024, Dec. 2016.

[38] J. Santamaría, O. Cordón, and S. Damas, "A comparative study of state-of-the-art evolutionary image registration methods for 3D modeling," *Computer Vision & Image Understanding*, vol. 115, no. 9, pp. 1340-1354, Sep. 2011.

[39] Li, P.; Wang, R.; Wang, Y.; Gao, G. Fast Method of Registration for 3D RGB Point Cloud with Improved Four Initial Point Pairs Algorithm. Sensors. 2020, 20(1): 138.

[40] Andrea Censi. On achievable accuracy for pose tracking. In Proceedings of the IEEE International Conference on Robotics and Automation (ICRA). Kobe, Japan, May 2009.

[41] Andrea Censi. An accurate closed-form estimate of ICP's covariance. In Proceedings of the IEEE International Conference on Robotics and Automation (ICRA), 3167–3172. Rome, Italy, April 2007.

[42] Jacopo Serafin, and Giorgio Grisetti, "Using Extended Measurements and Scene Merging for Efficient and Robust Point Cloud Registration," Robotics and Autonomous Systems (RAS), vol. 92, pp. 91-106, 2017.

[43] Jacopo Serafin, and Giorgio Grisetti. "NICP: Dense Normal Based Point Cloud Registration." To Appear In Proc. of the International Conference on Intelligent Robots and Systems (IROS), Hamburg, Germany, 2015.

[44] Jacopo Serafin, and Giorgio Grisetti. "Using Augmented Measurements to Improve the Convergence of ICP." In Proc. of the Int. Conf. on Simulation, Modeling and Programming for Autonomous Robots (SIMPAR), Springer, Bergamo, Italy, pp. 566-577, 2014.

[45] Igor Bogoslavskyi, Olga Vysotska, Jacopo Serafin, Giorgio Grisetti and Cyrill Stachniss. "Efficient traversability analysis for mobile robots using the kinect sensor." In Proc. of the European Conference on Mobile Robots (ECMR), Barcelona, Spain, pp. 158-163, 2013.

Peng Li received the Ph.D. degree in geodesy and survey engineering from China University of Science and Technology, Xuzhou, China, 2018. Since 2018, he has been an associate professor with the School of Geographic Information and Tourism, Chuzhou University, China. Since 2019, he has been a visiting scholar at the University of Calgary, Canada. His research interests include computer vision and laser scanning and data processing.

Ruisheng Wang is an Associate Professor in the Department of Geomatics Engineering at the University of Calgary which he joined in 2012. Prior to that, he worked as an industrial researcher at NOKIA in Chicago, USA since 2008. Dr. Wang holds a Ph.D. in Electrical and Computer Engineering from the McGill University, a M.Sc.E.in Geomatics Engineering from the University of New Brunswick, and a B.Eng. in Photogrammetry and Remote Sensing from the Wuhan University. His research interests include Geomatics and computer vision.

Yanxia Wang received the Ph.D. degree in geodesy and survey engineering from China University of Science and Technology, Xuzhou, China, 2015. Since 2017, she has been an associate professor with the School of Geographic Information and Tourism, Chuzhou University, China. Her research interests include computer vision and image processing.

Wuyong Tao received the master's degree from the East China Institute of Technology, Nanchang, China, in 2015. He is currently pursuing the Ph.D. degree from the School of Geodesy and Geomatics, Wuhan University, Wuhan, China. His research interests include laser scanning and data processing. Wuhan University, Wuhan, China. His research interests include laser scanning and data processing.